



Size-resolved source apportionment of particulate matter in urban Beijing during haze and non-haze episodes

S. L. Tian, Y. P. Pan, and Y. S. Wang

State Key Laboratory of Atmospheric Boundary Layer Physics and Atmospheric Chemistry (LAPC), Institute of Atmospheric Physics, Chinese Academy of Sciences, Beijing 100029, China

Correspondence to: Y. S. Wang (wys@mail.iap.ac.cn) and Y. P. Pan (panyuepeng@mail.iap.ac.cn)

Received: 14 January 2015 – Published in Atmos. Chem. Phys. Discuss.: 30 March 2015

Revised: 26 August 2015 – Accepted: 8 October 2015 – Published: 14 January 2016

Abstract. Additional size-resolved chemical information is needed before the physicochemical characteristics and sources of airborne particles can be understood; however, this information remains unavailable in most regions of China due to lacking measurement data. In this study, we report observations of various chemical species in size-segregated particle samples that were collected over 1 year in the urban area of Beijing, a megacity that experiences severe haze episodes. In addition to fine particles, high concentrations of coarse particles were measured during the periods of haze. The abundance and chemical compositions of the particles in this study were temporally and spatially variable, with major contributions from organic matter and secondary inorganic aerosols. The contributions of organic matter to the particle mass decreased from 37.9 to 31.2%, and the total contribution of sulfate, nitrate and ammonium increased from 19.1 to 33.9% between non-haze and haze days, respectively. Due to heterogeneous reactions and hygroscopic growth, the peak concentrations of the organic carbon, cadmium and sulfate, nitrate, ammonium, chloride and potassium shifted from 0.43 to 0.65 μm on non-haze days to 0.65–1.1 μm on haze days. Although the size distributions of lead and thallium were similar during the observation period, their concentrations increased by a factor of more than 1.5 on haze days compared with non-haze days. We observed that sulfate and ammonium, which have a size range of 0.43–0.65 μm , sulfate and nitrate, which have a size range of 0.65–1.1 μm , calcium, which has a size range of 5.8–9 μm , and the meteorological factors of relative humidity and wind speed were responsible for haze pollution when the visibility was less than 10 km. Source apportionment using Positive Matrix Factorization showed six $\text{PM}_{2.1}$ sources and seven $\text{PM}_{2.1-9}$

common sources: secondary inorganic aerosol (25.1% for fine particles vs. 9.8% for coarse particles), coal combustion (17.7% vs. 7.8%), biomass burning (11.1% vs. 11.8%), industrial pollution (12.1% vs. 5.1%), road dust (8.4% vs. 10.9%), vehicle emissions (19.6% for fine particles), mineral dust (22.6% for coarse particles) and organic aerosol (23.6% for coarse particles). The contributions of the first four factors and vehicle emissions were higher on haze days than non-haze days, while the reverse is true for road dust and mineral dust. The sources' contribution generally increased as the size decreased, with the exception of mineral dust. However, two peaks were consistently found in the fine and coarse particles. In addition, the sources' contribution varied with the wind direction, with coal and oil combustion products increasing during southern flows. This result suggests that future air pollution control strategies should consider wind patterns, especially during episodes of haze. Furthermore, the findings of this study indicated that the $\text{PM}_{2.5}$ -based data set is insufficient for determining source control policies for haze in China and that detailed size-resolved information is needed to characterize the important sources of particulate matter in urban regions and better understand severe haze pollution.

1 Introduction

Particulate matter (PM) is among the most important atmospheric pollutants that negatively affect human health and visibility. In addition, PM plays a significant role in global climate change and the nutrient cycle of ecosystem through its direct and indirect impacts (Huang et al., 2014; McFig-

gans, 2014; Pan et al., 2013). Due to rapid industrialization and urbanization in recent decades, China has become one of the most significant source regions for anthropogenic atmospheric emissions in the world (Guo et al., 2014). The Chinese capital of Beijing, a megacity with approximately 21 million inhabitants (Beijing statistical yearbook 2013), is experiencing extreme haze events (Sun et al., 2006). From 30 November to 2 December and from 7 to 8 December 2004, the highest concentration of PM_{2.5} (particulate matter with aerodynamic diameter lower than 2.5 μm) over 6 h was 329.8 μg m⁻³ (Sun et al., 2006). In addition, during the haze episode in January 2013, the highest instantaneous 5 min PM_{2.5} concentration was 770 μg m⁻³ at 20:48 local time (LT) on 12 January 2013 (Tian et al., 2014). Moreover, the highest instantaneous PM_{2.5} concentration reached 1000 μg m⁻³ in some heavily polluted areas of Beijing (Quan et al., 2014). Although previous studies have provided valuable information regarding the physical and chemical characteristics of PM in urban Beijing and its surrounding areas (Li et al., 2013; Du et al., 2014; Song et al., 2006; Chan et al., 2005; Schleicher et al., 2013; Sun et al., 2004), the factors that influence haze formation remain unclear due to its complexity (Yang et al., 2014; Jing et al., 2014). In addition, previous studies have primarily focused on single particle fractions, such as PM_{2.5}, and have neglected size-resolved chemical information, especially for coarse particles, which also play an important role in haze events (Tian et al., 2014; Sun et al., 2013).

Knowing the size distributions and associated chemical species is crucial for evaluating the effects of PM on human health, visibility and regional radiative forcing and for determining the sources, formation mechanisms and conversion processes of the particles (Pillai and Moorthy, 2001; Duarte et al., 2008; Liu et al., 2008; Contini et al., 2014). Typically, mass distribution of PM is dominated by three modes (or sub-modes): the condensation (~0.1–0.5 μm), droplet (~0.5–2 μm) and coarse (>2 μm) modes (Wang et al., 2012; Guo et al., 2010). Thus, to simplify mass distribution calculations in this study, the particle modes were defined as follows. The sizes of the condensation mode particles were between 0.43 and 0.65 μm, and the sizes of the droplet-mode particles were between 0.65 and 2.1 μm. Recent results have suggested that secondary sulfates and nitrates primarily formed in fine particles, with elevated concentrations in the droplet mode during haze days (Sun et al., 2013; Wang et al., 2012). During the extreme haze events in urban Beijing in early 2013, the peak mass concentration of particles shifted from 0.43–0.65 μm on clear days to 0.65–1.1 μm on lightly polluted days and 1.1–2.1 μm on heavily polluted days due to the hygroscopic growth of submicron particles and the formation of secondary particles, including organic carbon (OC) and sulfate (SO₄²⁻), nitrate (NO₃⁻) and ammonium (NH₄⁺) ions (Tian et al., 2014). Because long-term observations are lacking, it is unclear whether the peak shifts occurred dur-

ing other periods or whether this phenomenon only occurred during the extreme haze events in early 2013.

In addition, source apportionment based on size-fractionated PM data would provide additional insights regarding aerosol sources, especially during haze events (Pant and Harrison, 2012). For example, receptor models have been successfully used to identify coarse aerosol sources separately from fine aerosol sources (Karanasiou et al., 2009; Titos et al., 2014). Source apportionment studies have shown that the sources of PM₁₀ (particulate matter with aerodynamic diameter lower than 10 μm) and PM_{2.5} are different. Meanwhile, the features of sources and dominant sources during different pollution periods are different (Karanasiou et al., 2009; Vecchi et al., 2008), and understanding the sources of size-resolved chemical species (i.e., OC, SO₄²⁻, NO₃⁻ and NH₄⁺) is important for strategy-makers to effectively control and manage pollution (Hou et al., 2011; Zhang et al., 2014a; Fisher et al., 2011).

The main source apportionment methods can be divided into three categories: emissions inventory, diffusion model and receptor model. Among these categories, receptor models have been widely used because the methods are not limited by pollution discharge conditions, weather or terrain factors. The receptor models based on chemical analysis can be divided into two categories: one in which source profiles are needed, such as the Chemical Mass Balance method, and one in which source profiles are not needed, such as the Positive Matrix Factorization (PMF) method. Because it is difficult to build large and accurate source profiles, we use the PMF method to perform source apportionment in our study. Previously, source apportionment studies in Beijing have mainly focused on single size fractions (i.e., PM_{2.5}, PM₁₀). Overall, the results showed that the contributions of major sources to PM_{2.5} mass in Beijing exhibited seasonal and annual variations. The major sources of PM_{2.5} mass in Beijing during 2000 were dust (20%), secondary sulfate (17%), secondary nitrate (10%), coal combustion (7%), diesel and gasoline exhaust (7%), secondary ammonium (6%), biomass aerosol (6%), cigarette smoke (1%) and vegetative detritus (1%; Zheng et al., 2005). However, the PMF model identified six main sources of PM_{2.5} in 2009–2010: soil dust, coal combustion, biomass burning, traffic and waste incineration emissions, industrial pollution and secondary inorganic aerosols, with annual mean contributions of 16, 14, 13, 3, 28 and 26%, respectively (Zhang et al., 2013b). In addition, the PMF method resolved 87 and 80% of the PM_{2.5} in January and August 2004, respectively. The major sources were coal combustion (38% in January and 11% in August), secondary sulfate (9 and 24%), secondary nitrate (10 and 8%), biomass burning (15 and 1%), motor vehicle emissions (8 and 15%) and road dust (7 and 8%; Song et al., 2007). Previous studies regarding the size distributions of PM in urban Beijing have primarily focused on limited chemical species (Sun et al., 2013; Li et al., 2013; Yao et al., 2003) or have been con-

ducted over short periods (Li et al., 2012; Sun et al., 2010; Gao et al., 2012; Zhang et al., 2014b). To the best of our knowledge, no studies have been conducted on the source apportionment of size-resolved atmospheric particles based on long-term observations in urban Beijing.

To fill this knowledge gap, we observed size-resolved PM in urban Beijing from 1 March 2013 to 28 February 2014. In this study, we report the mass closure of particles based on a size-resolved chemical data set obtained from haze and non-haze days over four seasons. The PMF method was combined with back trajectory cluster analysis to estimate the relative contributions of sources in different size fractions between haze and non-haze days and among different regional sources. These results will help policy-makers design emission control strategies and can serve as a database for future field measurements and modeling studies.

2 Materials and methods

2.1 Sampling site

The experiment was performed from 1 March 2013 to 28 February 2014 at the Institute of Atmospheric Physics, Chinese Academy of Sciences (39°58' N, 116°22' E; Fig. S1 in the Supplement). The samplers were placed on the roof of a building approximately 8 m above the ground. The sampling site was located in northwest Beijing between the third and fourth ring roads. The site was selected to broadly represent the air pollution levels in urban Beijing because it was far from specific point emission sources.

2.2 Sampling collection

Two nine-stage samplers (Andersen Series 20-800, USA) with cutoff points of 0.43, 0.65, 1.1, 2.1, 3.3, 4.7, 5.8 and 9.0 μm , were used to simultaneously collect particles for 48 h (from 10:00 LT on Monday to 10:00 LT on Wednesday) every week at a flow rate of 28.3 L min^{-1} . Overall, 52 sets of size-resolved PM samples were respectively collected on quartz fiber filters and cellulose membranes (81 mm in diameter) during the study period. The quartz fiber filters were pre-fired (2 h at 800 °C) to remove all organic material and were weighed before and after sampling using a microbalance with a sensitivity of ± 0.01 mg. Filters were conditioned in a dryer at 25 ± 3 °C under a relative humidity (RH) of 22 ± 3 % for 72 h before each weighing. After re-weighing, the exposed filters were stored in a freezer at -20 °C to limit losses of volatile components loaded on the filters. To prevent the sampler from becoming blocked by particles during sampling, the samplers were cleaned using an ultrasonic bath for 30 min before each sampling. In addition, the sampling flow rates were calibrated before each sampling and were monitored using a flow meter during each sampling. Field blanks (a blank quartz filter and a blank cellulose membrane in each sampling) were used to determine any possible

background contamination. All of the tools used during sampling and analysis were cleaned, and the operator wore plastic gloves. Meanwhile, the meteorological parameters used in this study, including visibility, temperature, RH, wind speed (WS) and wind direction, were collected at Beijing Capital International Airport (<http://english.wunderground.com>; Fig. S2).

2.3 Chemistry analyses

A quarter of each quartz filter was subjected to extraction in 25 mL of deionized water (Millipore, 18.2 M Ω) in an ultrasonic bath for 30 min. The extraction liquid was filtered and subsequently measured using an ion chromatograph (DIONEX, ICS-90, USA) to determine the sodium (Na^+), NH_4^+ , potassium (K^+), magnesium (Mg^{2+}), calcium (Ca^{2+}), chloride (Cl^-), NO_3^- and SO_4^{2-} concentrations. For ion analysis, the ion chromatograph was equipped with a separation column (Ionpac CS12A 4 \times 250 mm for cations and Ionpac AS14A 4 \times 250 mm for anions) and a suppressor (CSRS 300 4 mm for cations and ASRS 300 4 mm for anions). The eluents used for cations and anions were 22 mmol L $^{-1}$ MSA and 3.5 mmol L $^{-1}$ Na_2CO_3 /1 mmol L $^{-1}$ NaHCO_3 , respectively. The ions were quantified by external standard curves every week, and one trace calibration standard solution was used to check the curve each day. The limit of detection was less than 0.02 $\mu\text{g m}^{-3}$ for all ions when the injection volume was 100 μL .

Using another quarter of each quartz filter, the concentrations of OC and elemental carbon (EC) were determined using a thermal/optical carbon aerosol analyzer (DRI Model 2001A, Desert Research Institute, USA). Briefly, a punch aliquot (0.495 cm 2) of a quartz fiber filter sample was heated stepwise in an oven at 140 °C (OC1), 280 °C (OC2), 480 °C (OC3) and 580 °C (OC4) under a pure helium atmosphere to volatilize the OC before heating to 580 °C (EC1), 740 °C (EC2) and 840 °C (EC3) in a 2 % oxygen-contained helium atmosphere for EC oxidation. At each stage, the formed CO_2 was catalytically converted to CH_4 by a MnO_2 catalyst, and the resulting CH_4 was measured using a flame ionization detector. The analyzer was calibrated before and after sample analysis by using a standard mixture of CH_4 and CO_2 . One sample was randomly selected from every 10 samples to conduct duplicate sample analyses. The measurement errors were less than 10 % for TC (OC+EC), and the OC and EC concentrations in the field blanks were less than 1 % of the sample levels and were subtracted from the samples.

A quarter of the cellulose membrane was digested in a mixture of concentrated HNO_3 (6 mL), HCl (2 mL) and HF (0.2 mL) in a closed vessel microwave digestion system (MARS5, CEM Corporation, Matthews, NC, USA). Then, an Agilent 7500ce inductively coupled plasma mass spectrometer (ICP-MS, Agilent Technologies, Tokyo, Japan) was used to determine the concentrations of 18 trace elements (Na, Mg, aluminum (Al), K, Ca, manganese (Mn), iron (Fe),

cobalt (Co), nickel (Ni), copper (Cu), zinc (Zn), molybdenum (Mo), cadmium (Cd), barium (Ba), thallium (Tl), lead (Pb), thorium (Th) and uranium (U)). A blank filter was analyzed in each batch for quality control. Quantitative analysis was conducted using external calibration standards with concentrations that were similar to those in the samples. In addition, internal standard elements (^{45}Sc , ^{72}Ge , ^{115}In and ^{209}Bi) were added online during the trace element analysis.

The analysis methods, information regarding the instruments used in this study (e.g., precision, calibration and detection limit) and quality control methods are described elsewhere (Pan and Wang, 2015; Li et al., 2012).

2.4 Chemical mass closure

Mass closure was used to discuss the relative contributions of the major components in the PM. The chemical species were divided into the following seven categories: sulfate–nitrate–ammonium (SNA), organic matter (OM), crustal materials (CM), heavy metals (HM), EC, sea salt (SS) and liquid water. The difference between the mass weighted by microbalance and that reconstructed using the above seven components was defined as unidentified matter. The calculation methods of the main components were described in our previous studies (Tian et al., 2014) and are shown in Table S1 in the Supplement for convenience.

2.5 PMF model

PMF is an effective source apportionment receptor model (Karanasiou et al., 2009; Bullock et al., 2008; Paatero and Tapper, 1994; Paatero, 1997). In this study, EPA-PMF 3.0 was applied separately for the fine (the input data included the mass concentrations and chemical species in the particles with sizes of <0.43 , 0.43 – 0.65 , 0.65 – 1.1 and 1.1 – 2.1 μm) and coarse (the input data included the mass concentrations and chemical species for particles with sizes of 2.1 – 3.3 , 3.3 – 4.7 , 4.7 – 5.8 and 5.8 – 9 μm) fractions. The number of samples analyzed for each of the fine and coarse fractions was 208. The chemical species included Na, Mg, Al, K, Ca, Mn, Fe, Co, Ni, Cu, Zn, Mo, Cd, Ba, Tl, Pb, Th, U, Na^+ , NH_4^+ , K^+ , Mg^{2+} , Ca^{2+} , Cl^- , SO_4^{2-} , NO_3^- , OC and EC. The uncertainty of the concentration data, which were also the input data, was calculated as shown below.

If the concentration is less than or equal to the provided method detection limit (MDL), the uncertainty is calculated using the following equation:

$$\text{uncertainty} = 5/6 \cdot \text{MDL}. \quad (1)$$

If the concentration is greater than the provided MDL, the calculation is

$$\text{uncertainty} = \sqrt{(\text{error fraction} \cdot \text{concentration})^2 + (\text{MDL})^2}. \quad (2)$$

In this study, the error fraction was estimated as 10 (the percent uncertainty multiplied by 100) for all of the chemical

species, and the MDLs were similar to those reported in previous studies (Li et al., 2012; Yang et al., 2009).

The base model was run 20 times with a different number of factors to obtain the best possible solution. During the first run, several species had a large number of absolute scaled residuals greater than 3, which indicated poor observed–predicted correlations. Then, these species were designated as “weak” and the model was rerun. When a reasonable solution was found, the bootstrapping technique was used to obtain the most meaningful results. Overall, 100 bootstrap runs were performed with a minimum r^2 value of 0.6. Of the 100 runs, the factors were mainly mapped to a base factor in every run, which indicated a stable result.

Several criteria are important for ensuring a good PMF solution. First, the modeled Q should be within 50% of the theoretical value. Second, the optimum number of factors should be determined by the criterion that each factor has a distinctively dominant grouping of compounds. Third, the model uncertainty produced by bootstrapping should be small. The principles are detailed elsewhere (Liu et al., 2014b; Titos et al., 2014; Moon et al., 2008).

2.6 Air mass back trajectory cluster

The 3-day backward trajectories arriving at the sampling site were calculated using the National Oceanic and Atmospheric Administration (NOAA) HYSPLIT 4 model with a $0.5^\circ \times 0.5^\circ$ latitude–longitude grid. The arrival level was set at 500 m above ground level (a.g.l.). The HYSPLIT model was run four times each day at starting times of 02:00, 08:00, 14:00 and 20:00 UTC during the sampling period. Then, all of the trajectories were divided into different groups based on the horizontal moving speed and direction of the air masses to form the trajectory clusters (Sirois and Bottenheim, 1995; Wang et al., 2006b).

3 Results

3.1 PM mass concentrations and chemical composition

Table 1 describes the concentrations of the size-resolved mass and chemical compositions during different seasons. The annual average concentrations of $\text{PM}_{2.1}$ (particulate matter with aerodynamic diameters less than 2.1 μm) and PM_9 (particulate matter with aerodynamic diameters less than 9 μm) were 67.3 and 129.6 $\mu\text{g m}^{-3}$, respectively. Although the present level of $\text{PM}_{2.1}$ is significantly lower than that in 2009–2010 (135 $\mu\text{g m}^{-3}$; Zhang et al., 2013b), it was more than 3 times higher than the National Ambient Air Quality Standard (NAAQS), which specifies an annual average $\text{PM}_{2.5}$ of 15 $\mu\text{g m}^{-3}$ (GB3095-2012, Grade I). In addition, PM_9 was approximately 3 times the NAAQS annual average PM_{10} of 40 $\mu\text{g m}^{-3}$ (Grade I). Thus, fine and coarse particles, defined in this study as particles with sizes <2.1 ($\text{PM}_{2.1}$) and

2.1–9.0 μm ($\text{PM}_{2.1-9}$), respectively, are important for PM in urban Beijing.

As shown in Table 1, the primary components of $\text{PM}_{2.1}$ are OC (24.5 % of $\text{PM}_{2.1}$), SO_4^{2-} (14.7 %), NO_3^- (11.2 %) and NH_4^+ (9.2 %). In contrast, Ca ($3.5 \pm 1.5 \mu\text{g m}^{-3}$), EC ($2.0 \pm 1.8 \mu\text{g m}^{-3}$) and other species in total accounted for approximately 40 % of $\text{PM}_{2.1}$. The composition of the coarse particles was different from that of the fine particles. In this study the highest contribution to $\text{PM}_{2.1-9}$ was Ca (16.3 % of $\text{PM}_{2.1-9}$), followed by OC (15.5 %), NO_3^- (4.5 %), Fe (4.1 %) and SO_4^{2-} (3.5 %). These species in total accounted for approximately 44 % of $\text{PM}_{2.1-9}$. The mass closure of size-resolved particles is discussed in detail below (Sect. 4.2).

3.2 Seasonality

The concentrations of $\text{PM}_{2.1}$ were greatest during winter (December to February, $76.8 \mu\text{g m}^{-3}$), followed by spring (March to May), summer (June to August) and autumn (September to November), with concentrations of approximately $65 \mu\text{g m}^{-3}$ during the latter three seasons (Table 1). In contrast, the concentrations of $\text{PM}_{2.1-9}$ decreased in the following order: spring > autumn > winter > summer.

The seasonal dependency varied by species. For most of the species that were enriched in the fine mode (with a $\text{PM}_{2.1} / \text{PM}_9$ chemical concentration ratio greater than 0.5, including NH_4^+ , Tl, Cd, Pb, SO_4^{2-} , NO_3^- , EC, K^+ , Zn, Cl^- , OC, Cu, Na, Na^+ , Mo and K), their $\text{PM}_{2.1}$ and $\text{PM}_{2.1-9}$ concentrations exhibited similar seasonal variations, with the $\text{PM}_{2.1}$ mass concentration being higher during colder seasons. However, the seasonal dependence of the concentration of certain species in $\text{PM}_{2.1}$ differs from the typical seasonal variation. For example, the concentrations of SO_4^{2-} and NH_4^+ in spring and summer were higher than those in autumn and winter. This result was consistent with the seasonal variability of SO_4^{2-} and NH_4^+ in $\text{PM}_{2.5}$ in 2009–2010 (Zhang et al., 2013b).

In addition, the OC concentrations in $\text{PM}_{2.1}$ decreased as follows: summer ($20.2 \mu\text{g m}^{-3}$) > spring ($16.5 \mu\text{g m}^{-3}$) > winter ($16.2 \mu\text{g m}^{-3}$) > autumn ($13.4 \mu\text{g m}^{-3}$). The high OC concentrations during the summer primarily resulted from the photochemical generation of more secondary organic carbon (SOC). This result can be confirmed by the OC/EC ratios, which exhibited the following seasonal pattern: summer (16.7) > spring (12.7) > autumn (6.7) > winter (4.9). Because EC primarily arises from primary combustion emissions, the OC/EC ratios were used to evaluate the contributions from SOC (Cao et al., 2007).

For species enriched in the coarse mode (with a $\text{PM}_{2.1} / \text{PM}_9$ chemical concentration ratio below 0.5, including Ni, Mn, U, Co, Mg^{2+} , Th, Al, Ba, Mg, Ca and Ca^{2+}), their $\text{PM}_{2.1}$ and $\text{PM}_{2.1-9}$ concentrations demonstrated typical seasonal variations, with higher concentrations observed during the spring and autumn (or winter) due to the in-

fluences of re-suspended soil dust. Re-suspended soil dust may result from both long transport dust and local anthropogenic sources (construction dust and mechanical abrasion processes). The relatively high wind speed during spring facilitated the ascent of road dust into the atmosphere and resulted in the relatively high value of the species in the coarse mode (Liu et al., 2014a).

3.3 Size distribution

The size distributions of the mass concentrations and the chemical species are shown in Figs. 1 and S3. In each season, the size distribution of the mass concentrations was bimodal. The fine modes commonly showed maxima at 0.65–1.1 μm in spring, autumn and winter and 0.43–0.65 μm in summer. The coarse modes showed maxima at 4.7–5.8 μm in all of the seasons. As shown in Fig. 1, the peak of the fine mode was broader in winter than in the other seasons, indicating the complexity of the emissions in winter (Sun et al., 2013). Emissions from coal combustion for heating are greater during winter, especially for retail coal combustion in surrounding areas, which is difficult to control (Wang et al., 2006a). However, the meteorological conditions in winter are unfavorable for the diffusion of fine particles and precursors (SO_2 , NO_x , volatile organic compounds (VOCs)), making secondary particle emissions more complex.

The chemical species can generally be divided into three groups based on their size distributions. First, SO_4^{2-} , NO_3^- , NH_4^+ , EC, Zn, Cd, Pb and Tl were abundant in the fine mode, which exhibited maxima at 0.43–0.65 or 0.65–1.1 μm in all four seasons that corresponded to coal and motor vehicle sources (Li et al., 2013). Second, Ca^{2+} , Mg^{2+} , Ba, Mg, Al, Ca, Fe, Co, Ni, Th and U were primarily concentrated in the coarse mode from 4.7 to 5.8 μm , which suggested natural sources from soil dust or mechanical abrasion processes (Sun et al., 2013; Maenhaut et al., 2002). Third, OC, Cl^- , K^+ , Na^+ , Na, K, Mn, Cu and Mo exhibited typical bimodal distributions, and the amplitude of the fine mode was well correlated with that of the coarse mode. These species exhibited maxima at 0.43–0.65 or 0.65–1.1 μm and peaked at 4.7–5.8 μm in the coarse mode. Cl^- and K^+ are good biomass burning tracers (Du et al., 2011), and Mn and Cu are good industrial pollution tracers. Hence, the species in the third group may represent mixed sources from biomass burning and industrial pollution.

The size distribution of the mass concentration and OC peaked at 0.43–0.65 in summer and 0.65–1.1 μm in winter. Because the primary organic carbon emissions were relatively stable across the four seasons, the size distribution differences in the fine mode primarily resulted from the generation of SOC (Duan et al., 2005). The difference between summer and winter indicated that the SOC formation in summer was enhanced due to photochemical reactions and primarily accumulated in “condensation mode” (Zhang et al., 2008). However, because photochemistry is typically weak in win-

Table 1. Concentrations of different chemical compositions in size-resolved particles during entire sampling period (annual) and four seasons ($\mu\text{g m}^{-3}$).

Size	Annual		Spring		Summer		Autumn		Winter	
	PM _{2.1}	PM _{2.1-9}								
Mass	67.27	62.33	64.65	68.05	65.05	57.97	62.52	62.87	76.84	60.41
OC	16.50	9.63	16.26	10.44	20.19	16.68	13.40	6.76	16.16	4.64
EC	2.01	0.77	1.28	0.71	1.47	0.81	1.99	0.82	3.32	0.75
Na ⁺	0.79	0.66	0.48	0.57	0.27	0.31	1.67	0.92	0.74	0.82
NH ₄ ⁺	6.17	0.70	8.00	0.74	6.11	0.41	4.65	0.56	5.92	1.08
K ⁺	0.72	0.29	0.83	0.49	0.33	0.12	0.60	0.09	1.12	0.46
Mg ²⁺	0.21	0.40	0.30	0.41	0.14	0.36	0.20	0.42	0.20	0.40
Ca ²⁺	1.01	3.38	1.25	3.98	0.67	2.69	1.00	3.77	1.10	3.08
Cl ⁻	1.58	0.81	1.98	1.19	0.17	0.31	1.23	0.46	2.95	1.28
NO ₃ ⁻	7.51	2.78	8.51	3.56	4.08	2.33	6.60	2.46	10.84	2.76
SO ₄ ²⁻	9.87	2.17	11.02	2.80	10.02	1.47	9.28	2.08	9.16	2.35
Na	1.78	1.34	1.77	1.33	1.81	1.12	1.81	1.29	1.73	1.64
Mg	0.45	1.19	0.51	1.63	0.49	1.08	0.46	1.14	0.35	0.91
Al	0.65	1.39	0.73	2.06	0.60	0.90	0.69	1.32	0.59	1.29
K	0.69	0.62	0.88	0.98	0.49	0.49	0.74	0.59	0.65	0.42
Ca	3.54	10.17	4.03	16.31	4.63	10.20	3.21	8.63	2.30	5.55
Mn	0.04	0.04	0.05	0.06	0.03	0.03	0.04	0.04	0.03	0.04
Fe	1.23	2.58	1.55	3.66	1.43	2.08	1.36	2.62	0.58	1.98
Co	0.001	0.001	0.001	0.001	0.001	0.001	0.001	0.001	0.001	0.001
Ni	0.013	0.014	0.011	0.012	0.014	0.010	0.014	0.018	0.014	0.015
Cu	0.026	0.020	0.030	0.020	0.015	0.015	0.029	0.022	0.029	0.023
Zn	0.21	0.10	0.24	0.12	0.18	0.09	0.23	0.09	0.19	0.09
Mo	0.006	0.006	0.002	0.001	0.002	0.002	0.002	0.001	0.002	0.002
Cd	0.001	0.000	0.001	0.000	0.001	0.000	0.001	0.000	0.001	0.000
Ba	0.017	0.043	0.018	0.057	0.014	0.032	0.018	0.044	0.017	0.039
Tl	0.001	0.000	0.001	0.000	0.001	0.000	0.001	0.000	0.001	0.000
Pb	0.089	0.018	0.094	0.022	0.071	0.013	0.088	0.015	0.103	0.022
Th	0.000	0.000	0.000	0.001	0.000	0.000	0.000	0.000	0.000	0.001
U	0.000	0.000	0.000	0.000	0.000	0.000	0.000	0.000	0.000	0.000

ter, the SOC generation mainly resulted from the high RH and high precursor concentrations, including VOCs from biological and anthropogenic sources (Jacobson et al., 2000). Thus, VOCs primarily accumulated in “droplet mode” (Cao et al., 2007). Previously, our findings indicated that weakening incident solar radiation reduces the formation of SOC formation in the $< 1.1 \mu\text{m}$ size fraction and that high RH plays an important role in the generation of SOC in $1.1\text{--}2.1 \mu\text{m}$ size fraction (Tian et al., 2014).

3.4 Ion balance

We calculated the ion balance for each size fraction, which was used to evaluate the ion deficiency between cations and anions in the PM (Fig. S4). The average equivalent ratio of total cations (Na⁺, NH₄⁺, K⁺, Mg²⁺ and Ca²⁺) to total anions (SO₄²⁻, NO₃⁻ and Cl⁻) ranged from 0.95 to 2.50, with the lowest ratio occurring in the $1.1\text{--}2.1 \mu\text{m}$ size fraction and the highest ratio occurring in the $4.7\text{--}5.8 \mu\text{m}$ size fraction. The total cation to total anion ratio in the fine particles

was near unity throughout the year, which indicated excellent charge balance and high data quality. The slope for the fine mode particles was mainly greater than 1 because the concentrations of CO₃²⁻ and HCO₃⁻ were not determined.

Figure S5 shows good correlations between the NH₄⁺ and SO₄²⁻ concentrations in the fine particles for the data sets in different seasons, with NH₄⁺ / SO₄²⁻ equivalent ratios greater than 1 (spring (1.92), summer (1.79), autumn (1.01), winter (1.36)), revealing the dominance of (NH₄)₂SO₄. Next, we calculated the molar ratio of NH₄⁺ to [NO₃⁻ + SO₄²⁻], which was slightly higher than unity in spring (1.25) and summer (1.33) and indicated the presence of NH₄NO₃ in the fine aerosols. However, the ratios were less than 1 in the autumn (0.78) and winter (0.68), which indicated that NO₃⁻ could be present in chemical forms other than NH₄NO₃.

For the coarse mode particles, the NH₄⁺ / SO₄²⁻ equivalent ratios in spring (0.78), summer (0.68) and autumn (0.58) were less than 1 but greater than 0.5, which indicated the dominance of (NH₄)₂SO₄ and NH₄HSO₄. By contrast, the

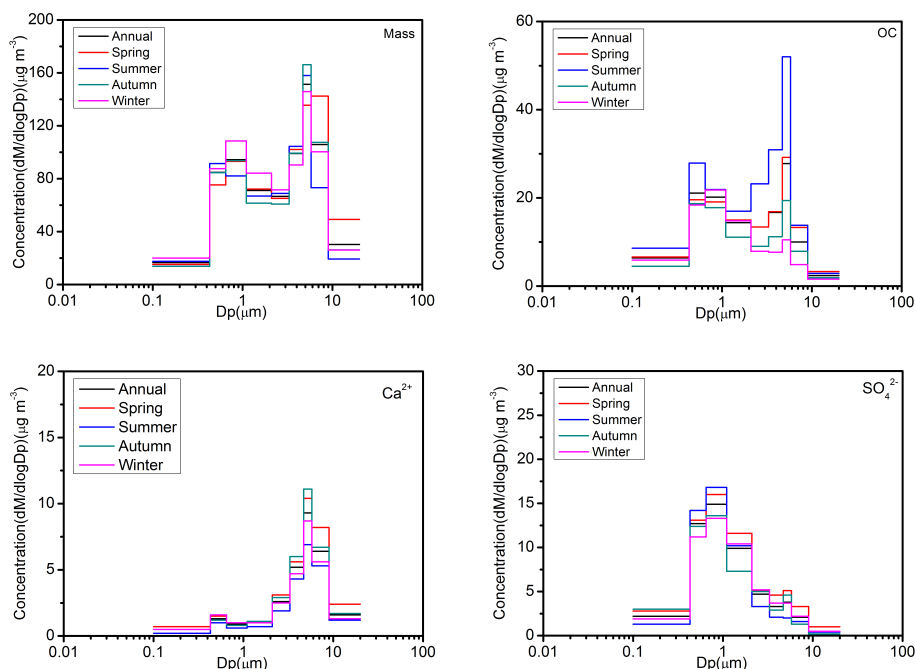


Figure 1. Mass concentration size distributions and those of typical chemical species in different categories.

ratio in winter (1.33) was greater than unity, and the equivalent ratio of NH_4^+ to $[\text{NO}_3^- + \text{SO}_4^{2-}]$ in winter was less than unity.

4 Discussion

4.1 Size-resolved aerosol compositions on non-haze and haze days

Figure 2 illustrates the size-segregated PM mass concentrations during the sampling period. Haze is defined as a weather phenomenon in which a high concentration of fine particles occur that result in a visibility of less than 10 km at an RH of less than 90 % (Sun et al., 2006; Tan et al., 2009; Zhuang et al., 2014). Thus, we used visibility and RH to determine the haze/no-haze days as follows: sampling days with visibility < 10 km and RH < 90 % were defined as haze days and sampling days with visibility > 10 km and RH < 90 % were defined as non-haze days. During the observation period, 12 sets of size-resolved PM samples were collected during non-haze days and 19 sets were collected during haze days (marked in Fig. 2). Of the remaining 21 sets, 15 sets were collected during rain, snow or fog days and 6 sets were collected during dust days (visibility < 10 km, RH < 40 %). These samples were excluded from the data set when we discussed the differences between haze and non-haze days.

4.1.1 Concentration enhancement ratios

Table S2 describes the annual average concentrations of the size-resolved mass and chemical compositions on haze and non-haze days over four seasons. The annual average $\text{PM}_{2.1}$ and $\text{PM}_{2.1-9}$ concentrations on haze days were 86.1 and $72.6 \mu\text{g m}^{-3}$, which were 2.6 and 1.4 times those on non-haze days, respectively. Therefore, it is evident that fine particles significantly accumulated during the haze pollution period (Wang et al., 2014). In addition, the mass concentration enhancement ratio from non-haze to haze days ($R_{H/N}$) was examined during all four seasons.

$$R_{H/N} = C_H/C_N, \quad (3)$$

where C_H is the concentration of chemical species on haze days and C_N is the concentration of chemical species on non-haze days.

The $R_{H/N}$ for fine particles revealed a typical seasonality, with the highest value occurring in winter (5.6) and the lowest value occurring in the spring (1.8). The $R_{H/N}$ for coarse particles was lower than that for fine particles, which ranged from 1.1 to 1.9 and decreased as follows: summer > autumn > winter > spring. The higher $R_{H/N}$ values for fine particles further indicated the importance of fine particles in haze pollution.

We calculated the $R_{H/N}$ ratios for chemical species in each size fraction. Based on the pattern of $R_{H/N}$ ratios that varied with increasing size fraction, all of the species can be divided into three groups. First, OC, NO_3^- , SO_4^{2-} , NH_4^+ , K^+ , Cl^- , K, Mn, Ni, Cu, Zn, Pb and Tl exhibited high $R_{H/N}$ ratios in

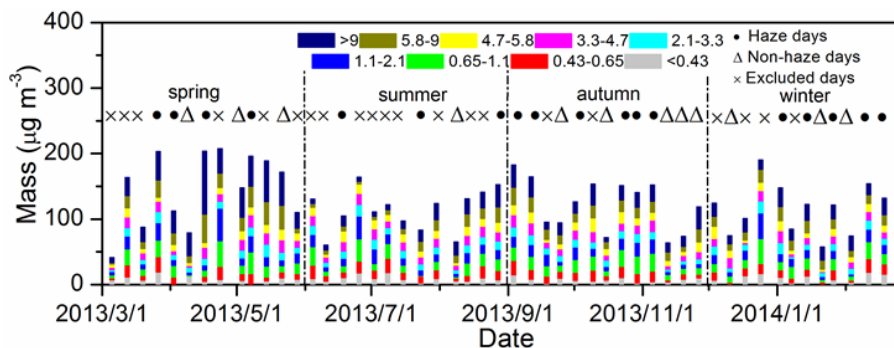


Figure 2. Size-resolved mass concentration (distributions that are marked as solid circle and open triangle denote haze and non-haze days, respectively).

fine mode and a peak value in size fraction 0.65–1.1 or 1.1–2.1 μm . Second, $R_{\text{H/N}}$ ratios of Na^+ , Mg^{2+} , Ca^{2+} , Mg and Fe increased with increasing size fraction. Third, the $R_{\text{H/N}}$ ratios of EC , Na , Al , Ca , Co , Mo , Cd , Ba , Th and U first increased and then decreased with increasing size fraction and exhibited highest $R_{\text{H/N}}$ ratios in size fraction 1.1–2.1, 2.1–3.3 or 3.3–4.7 μm .

The annual average $R_{\text{H/N}}$ of the chemical components in $\text{PM}_{2.1}$ ranged from 0.8 to 5.5, with values greater than 2.6 for NO_3^- , SO_4^{2-} , NH_4^+ , Pb , Tl and Cd . This finding was consistent with the findings of previous studies (Tian et al., 2014; Sun et al., 2013), indicating that coal and motor vehicle sources played important roles in haze pollution (Li et al., 2013). Regarding the seasonal variations, the particulate mass and most of the species exhibited the highest $R_{\text{H/N}}$ in winter, which indirectly showed that severe haze events primarily occurred in winter.

Simultaneously, the annual average $R_{\text{H/N}}$ of the chemical components in $\text{PM}_{2.1-9}$ ranged from 0.8 to 5.3, which was similar to that for fine particles. The NH_4^+ , NO_3^- , SO_4^{2-} , Cd , EC , Cl^- , Pb , Tl , Na^+ , OC , Zn and K^+ in the coarse fraction exhibited $R_{\text{H/N}}$ values greater than 1.4. Among these species, Pb , Cd and Tl had high toxicity. Thus, the mitigation of particles with diameters greater than 2.1 μm cannot be neglected during haze events. Similar to $\text{PM}_{2.1}$, most of the species in the coarse fraction exhibited the highest $R_{\text{H/N}}$ in winter. In contrast, the highest $R_{\text{H/N}}$ values for Na^+ , K^+ and Cl^- in the coarse fraction were observed in summer, which was similar to the results of the mass concentration. The highest $R_{\text{H/N}}$ for Na^+ , K^+ and Cl^- in the coarse fraction was observed in summer, mainly due to low concentrations on non-haze days and relatively high concentration of haze days. The lower concentrations of coarse particles in summer were likely related to greater precipitation during this season. High concentrations of K^+ and Cl^- in coarse mode on haze days were mainly associated with biomass burning (Du et al., 2011). One of the samples that represented a haze day in summer was collected between 17 and 19 June. During this period, burning wheat straw in the surrounding areas affected

both fine and coarse particle pollution in Beijing (Wang et al., 2015; Yan et al., 2015; Cheng et al., 2014).

The concentrations of NO_3^- , SO_4^{2-} and NH_4^+ in the fine and coarse particles were higher on haze days than on non-haze days. These species are involved in heterogeneous chemical reactions (Sun et al., 2013). Figure S6a and b show good correlations between NH_4^+ and SO_4^{2-} in fine particles from non-haze and haze days, with an equivalent $\text{NH}_4^+ / \text{SO}_4^{2-}$ ratio greater than unity (ranging from 1.5 to 1.6). This result reveals the dominance of $(\text{NH}_4)_2\text{SO}_4$. Next, we calculated the equivalent ratio of NH_4^+ to $[\text{NO}_3^- + \text{SO}_4^{2-}]$ (Fig. S6c and d), which was slightly higher than unity on non-haze days and indicated the presence of NH_4NO_3 in the fine mode aerosols. However, on haze days, the ratios were less than unity, which indicated that NO_3^- may be present in chemical forms other than NH_4NO_3 .

4.1.2 Peak shifts

Figure 3 compares the annual average mass concentration size distributions on non-haze and haze days, which were considered bimodal, with the peaks corresponding to the fine modes located at 0.65–1.1 μm and those corresponding to the coarse modes peaking at 4.7–5.8 μm . No significant differences in the average size distributions were found between haze and non-haze days in each season (Fig. 3). This result was inconsistent with the results obtained from early 2013, which showed that the peak mass concentration of fine mode particles shifted from 0.43–0.65 μm on clear days to 0.65–1.1 μm on lightly polluted days and 1.1–2.1 μm on heavily polluted days (Tian et al., 2014). During previous haze pollution events in Beijing, a continuous growth of the nucleation mode particles was also clearly depicted by the evolution in the mean particle size, which increased from about 40 nm when the $\text{PM}_{2.5}$ level was less than $50 \mu\text{g m}^{-3}$ to about 190 nm when the $\text{PM}_{2.5}$ concentration exceeded $300 \mu\text{g m}^{-3}$ over the course of 3 days (Guo et al., 2014).

However, in this study, peak shifts from 0.43–0.65 μm on non-haze days to 0.65–1.1 μm on haze days were observed

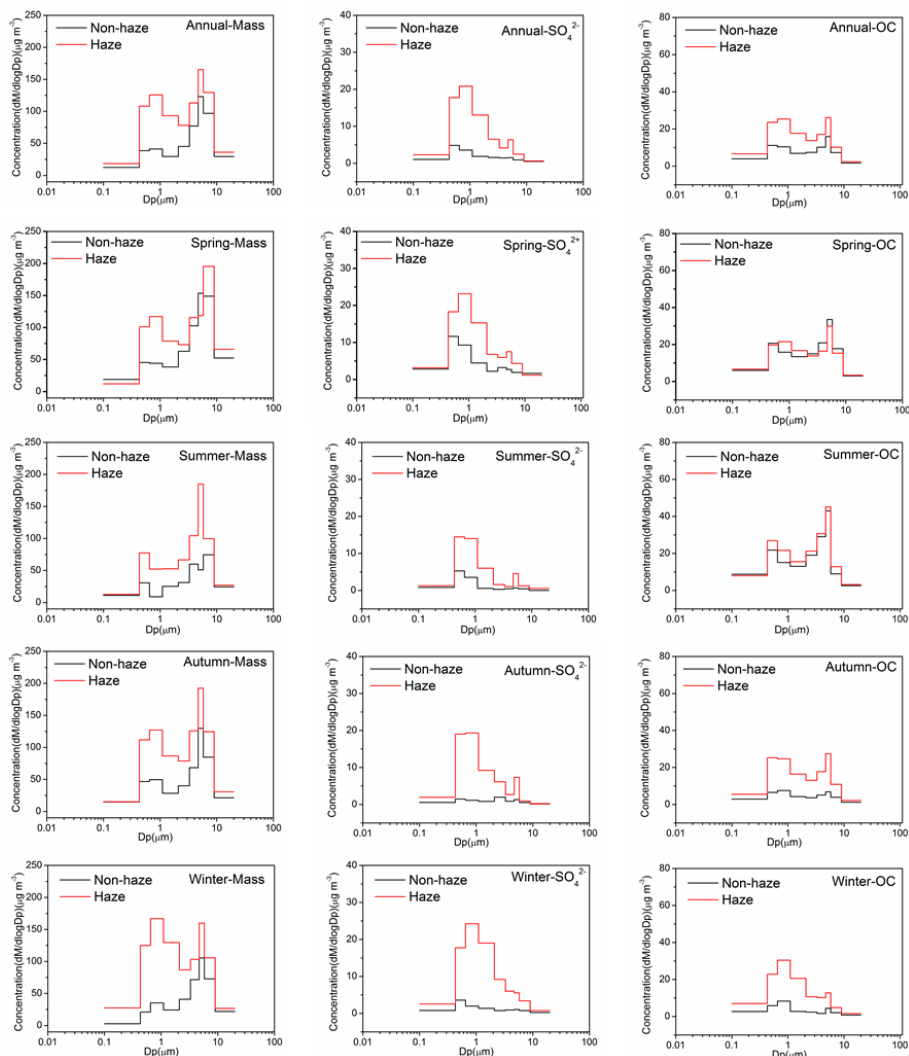


Figure 3. Mass concentration size distributions on haze and non-haze days over the entire sampling period (annual) and by season as well as those of the typical chemical species.

when considering the annual average size distributions of SO_4^{2-} , OC, NO_3^- , NH_4^+ , Cl^- , K^+ and Cd. The peak values of these species at 0.43–0.65 μm in the fine mode on non-haze days correspond to the “condensation mode” due to the transformation of precursors and heterogeneous reactions, while those at 0.65–1.1 μm on haze days correspond to the “droplet mode”, which likely form in clouds or through aqueous-phase chemical reactions (Sun et al., 2013). The high RH during haze days may facilitate the formation of “droplet mode” particles, and a similar finding was previously reported (Sun et al., 2013; Zhang et al., 2013a). However, this result was slightly different from that observed in early 2013, which showed that the peak concentration of NH_4^+ , SO_4^{2-} and NO_3^- in fine mode at 1.1–2.1 μm on heavily polluted days resulted from the high RH and high precursor concentrations (Tian et al., 2014).

We also compared size distributions of chemical species between haze and non-haze days in different seasons. The results showed that the peak concentration of OC, SO_4^{2-} , Cl^- and Mn in fine mode particles shifted from 0.43–0.65 μm on non-haze days to 0.65–1.1 μm on haze days in spring. However, the species that exhibited peak shifts in summer were EC, K^+ , NO_3^- and Ni. Besides, in autumn, fine mode peak concentration of EC, NH_4^+ , SO_4^{2-} , NO_3^- , Cd and Cu shifted from 0.43–0.65 μm on non-haze days to 0.65–1.1 μm on haze days. Meanwhile, NH_4^+ , SO_4^{2-} , NO_3^- , K^+ , Cl^- , Cd, Zn and Pb exhibited fine mode peak shifts from non-haze days to haze days in winter. These results indicate that there are different formation mechanisms for haze in different seasons.

4.2 Mass closure studies

4.2.1 Non-haze vs. haze days

Mass closure studies showed that SNA, OM and CM dominated the fine particles, which accounted for 87.7 and 76.6 % of the $PM_{2.1}$ mass on non-haze and haze days, respectively (Fig. 4a–d). Generally, the contribution of OM to $PM_{2.1}$ was greater than the contributions of SNA and CM. However, during haze episodes in cold seasons, SNA was more significant than OM because the high RH and precursor emissions (i.e., SO_2) promoted the generation of SNA (Tian et al., 2014). OM dominated in fine particles and decreased from 37.9 % on non-haze days to 31.2 % on haze days. Such an observation may reflect two distinct processes occurring during haze formation in Beijing. New particle formation has been found to be prevalent in Beijing during clean period and the nucleation mode particles contained mainly secondary organics (Guo et al., 2014). Nucleation consistently precedes a polluted period, producing a high number concentration of nano-sized particles under clean conditions and the growth process competes with capture/removal of nanoparticles by coagulation with preexisting aerosols. In addition, there is also much evidence showing that organics play a key role in new particle formation, both in the enhancement of aerosol nucleation and in the growth of freshly nucleated particles. For example, the interaction between organic and sulfuric acids promotes efficient formation of organic and sulfate aerosols in the polluted atmosphere (Zhang et al., 2004; Zhang et al., 2011). In contrast, the contribution of SNA to the $PM_{2.1}$ mass increased from 19.1 % on non-haze days to 33.9 % on haze days, indicating that SNA played a key role in haze formation. For haze pollution that is associated with high RH, the aqueous phase on the aerosol surface provides a means for the rapid heterogeneous gas–liquid conversion of gaseous precursors to produce secondary inorganic aerosols (Wang et al., 2012; Zhang et al., 2015b).

High total CM, OM and SNA contributions were also observed in $PM_{2.1-9}$, which accounted for 58.5 and 54.3 % of the total $PM_{2.1-9}$ mass on non-haze days and haze days, respectively. The contributions of these species in coarse particles decreased as follows on haze and non-haze days: CM > OM > SNA. However, in fine particles, the order was OM > CM > SNA on non-haze days and OM > SNA > CM on haze days. In summary, the relative contributions of OM and CM to the particle mass decreased from non-haze to haze days, and the relative contribution of SNA increased from non-haze days to haze days. Similar trends had been observed in previous Beijing haze study (Guo et al., 2014), in which the organic mass fraction dominates in the clean period (74–77 %) and decreases slightly during the transition (48–49 %) and polluted (35–42 %) periods. The contributions of sulfate and nitrate to the particle mass concentration increase throughout the pollution period from mass fractions

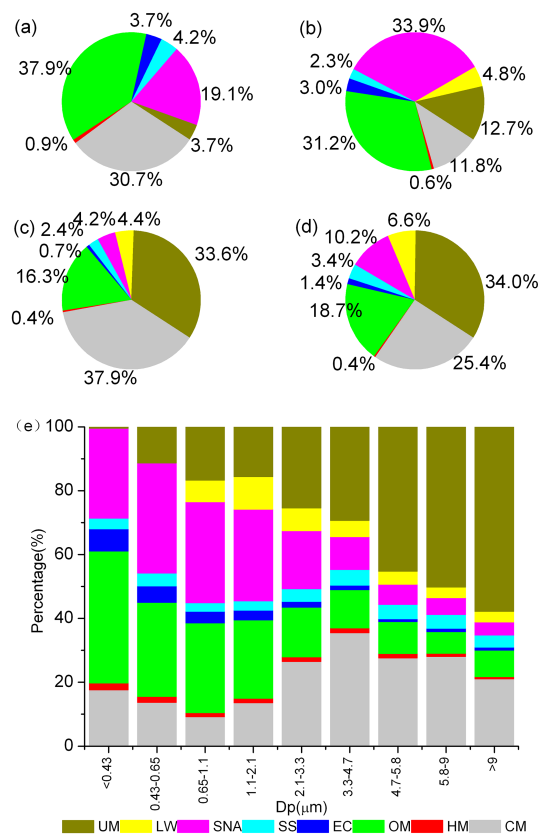


Figure 4. Contributions of different components to the total masses in (a) $PM_{2.1}$ on non-haze days, (b) $PM_{2.1}$ on haze days, (c) $PM_{2.1-9}$ on non-haze days, (d) $PM_{2.1-9}$ on haze days and (e) different size fractions.

of 8–9 and 6–12 % for the clean period to 23–26 and 12–27 % for the polluted period, respectively.

4.2.2 Differences among size fractions

For different size fractions, the contributions of OM, HM and EC were greatest in the $<0.43 \mu\text{m}$ fraction (41.3, 2.2 and 7.0 %, respectively). The contribution of SNA, which is primarily formed from precursors via heterogeneous reactions, was greatest in the $0.43\text{--}0.65 \mu\text{m}$ fraction (34.5 %), which is within the “condensation mode” (Fig. 4e). The contribution decreased as the size increased, which indicated that these anthropogenic species primarily accumulated in the fine mode. However, the minimal contributions of OM, HM, EC and SNA occurred in the $5.8\text{--}9 \mu\text{m}$ (6.9 %), $>9 \mu\text{m}$ (0.7 %), $4.7\text{--}5.8 \mu\text{m}$ (0.9 %) and $>9 \mu\text{m}$ (4.1 %) size fractions, respectively. In addition, CM and SS exhibited similar size fraction variations, which increased from $<0.43 \mu\text{m}$ to $3.3\text{--}4.7 \mu\text{m}$ and then decreased. The highest contributions of CM and SS appeared in the $3.3\text{--}4.7 \mu\text{m}$ fraction and were 35.6 and 4.9 %, respectively.

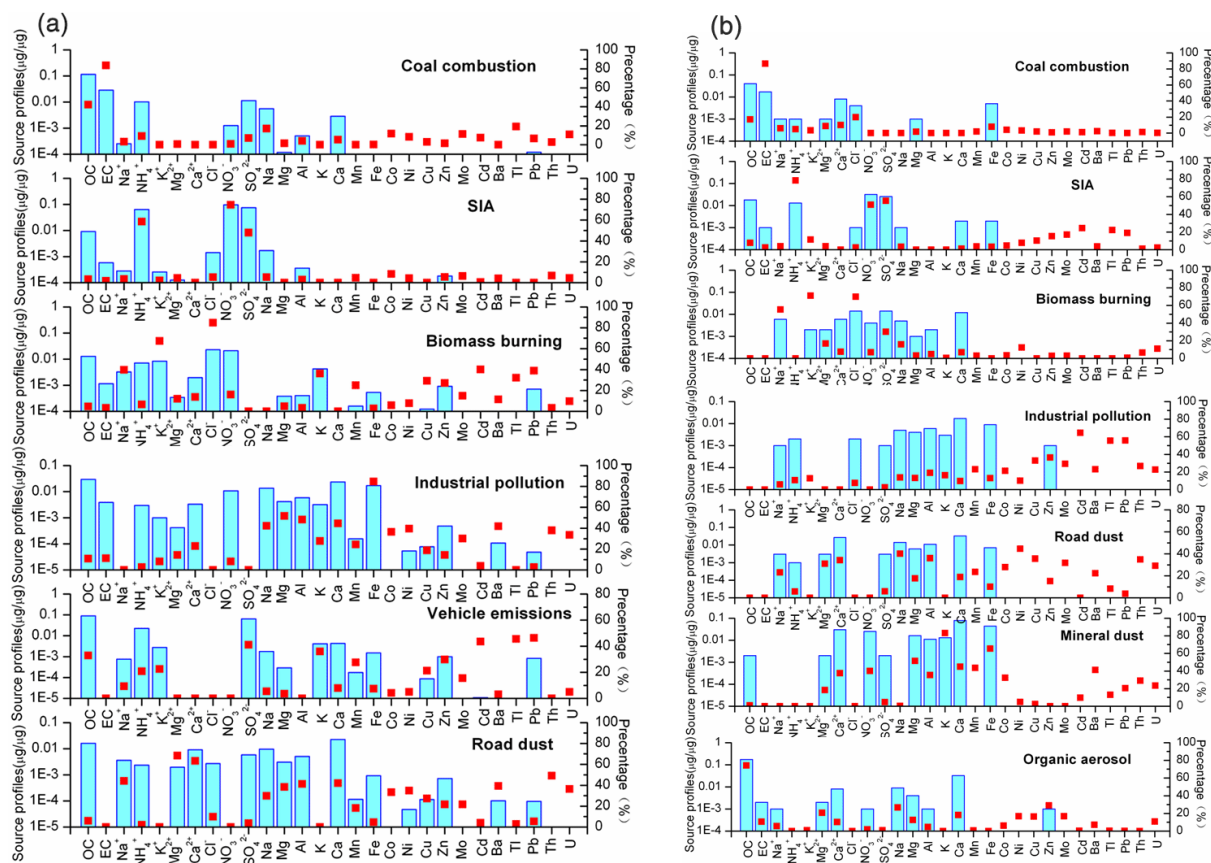


Figure 5. The profiles of each source in (a) fine and (b) coarse fractions.

4.2.3 Unidentified mass

The reconstructed PM mass concentrations were compared with the gravimetric values, as shown in Fig. S7. The results were correlated with one another in the different size fractions, with R^2 values for $PM_{1.1}$ (particulate matter with aerodynamic diameter lower than $1.1 \mu\text{m}$), $PM_{2.1}$, PM_9 and total suspended particulate matter of 0.69, 0.79, 0.70 and 0.60, respectively. In addition, the contributions of the unidentified components ranged from 0.4 to 57.8 % and increased as the sizes increased. The large unidentified components in the coarse particles potentially resulted from underestimating CM (Hueglin et al., 2005; Sun et al., 2004). In this study, Si was estimated as 3.42 times Al, and the ratios were applied to all of the size fractions. This assumption may be underestimated because the Si / Al ratio could increase with size. For example, the contribution of CM to coarse particles reached 42.4 % based on the Si / Al ratio of 6.0 in $PM_{2.5-10}$, which was previously reported in Beijing (Zhang et al., 2010). Thus, the contribution of the unidentified components decreased from 38.5 to 25.5 % for the total $PM_{2.1-9}$ mass.

4.3 Source apportionment

4.3.1 Fine and coarse particles

Six $PM_{2.1}$ and seven $PM_{2.1-9}$ sources were identified by PMF analysis. Figure 5a and b show the profiles of each source in the fine and coarse fractions, respectively, and the percentages of species apportioned by each source. The sources identified in the fine fraction were named as secondary inorganic aerosol (SIA), coal combustion, biomass burning, industrial pollution, road dust and vehicle emissions. Coarse fraction sources were SIA, coal combustion, biomass burning, industrial pollution, road dust, mineral dust and organic aerosol. Together these sources represented 91.6 and 86.6 % of $PM_{2.1}$ and $PM_{2.1-9}$, respectively.

Secondary inorganic aerosol

The first source was relevant to SIA, which was identified in both fine and coarse fractions and was typically characterized by significant amounts of SO_4^{2-} , NO_3^- and NH_4^+ . SIA contributed 25.1 % ($16.9 \mu\text{g m}^{-3}$) and 9.8 % ($6.1 \mu\text{g m}^{-3}$) to the fine and coarse particles, respectively. Contributions of SIA to both $PM_{2.1}$ and $PM_{2.1-9}$ followed the order winter (29.5 % to $PM_{2.1}$ and 16.5 % to $PM_{2.1-9}$) > spring (27.2 and 9.3 %)

> autumn (20.3 and 7.8 %) > summer (18.1 and 5.7 %). The SIA contribution to the fine particles was similar to that in Beijing for 2009–2010 (Zhang et al., 2013b).

Coal combustion

The second source, coal combustion, was also identified in both fine and coarse fractions and was characterized by elevated OC and EC concentrations (Tian et al., 2010; Kang et al., 2011). The contribution of this source to $PM_{2.1}$ was 17.7 % ($11.9 \mu\text{g m}^{-3}$), which closely approximates the value of 19 % derived in Beijing for 2009–2010 (Zhang et al., 2013b). In addition to its contribution to $PM_{2.1}$, coal combustion significantly contributed to $PM_{2.1-9}$ (7.8 %, $4.9 \mu\text{g m}^{-3}$). The contributions of coal combustion to $PM_{2.1}$ and $PM_{2.1-9}$ exhibited similar seasonal patterns of winter (27.0 % to $PM_{2.1}$ and 9.4 % to $PM_{2.1-9}$) > autumn (17.5 and 8.9 %) > summer (14.5 and 6.6 %) > spring (9.6 and 6.4 %).

Biomass burning

The third source, biomass burning, was also identified in both fractions and was represented by high Cl^- and K^+ contents (also K, which is an excellent tracer of aerosols from biomass burning; Du et al., 2011) and was rich in Na^+ (Moon et al., 2008). The contribution of this source to $PM_{2.1}$ was 8.6 %, which was slightly higher than that to $PM_{2.1-9}$ (6.9 %). This finding is expected because biomass burning contributed much more to the fine particles than the coarse particles (Cheng et al., 2014). Its contributions to $PM_{2.1}$ and $PM_{2.1-9}$ demonstrated a typical seasonal variation, with higher values in spring (11.1 % to $PM_{2.1}$ and 11.8 % to $PM_{2.1-9}$) and winter (13.5 and 10.2 %).

Industrial pollution

The fourth source was industrial pollution, which was also identified in both fine and coarse fractions and was characterized by high Fe, Ni, Co, Mg, Al and Ca contents in fine size fraction and by high Cd, Pb, Tl, Zn and Cu contents in coarse fraction (Karnae and John, 2011). The contribution from this source was 12.1 %, which is significantly higher than the 5.1 % contribution for coarse particles. Its contributions to $PM_{2.1}$ and $PM_{2.1-9}$ demonstrated a typical seasonal variation, with higher values in summer (16.7 %) and autumn (14.5 %) for fine fraction and with higher values in winter (5.7 %) and spring (7.9 %) for coarse fraction.

Road dust

The fifth component, road dust, was also identified in both fine and coarse fractions and was related to the high loading of crustal elements, such as Al, Ca (Ca^{2+}), Mg (Mg^{2+}), Na (Na^+), Co, Ni and Cu (Titos et al., 2014; Vecchi et al., 2008). This source represented 8.4 and 10.9 % of the total mass in the fine and coarse fractions, respectively. Contributions

of road dust to both $PM_{2.1}$ and $PM_{2.1-9}$ followed the order winter (9.9 % to $PM_{2.1}$ and to 18.3 % to $PM_{2.1-9}$) > autumn (10.2 and 16.0 %) > spring (4.9 and 9.3 %) > summer (6.3 and 4.7 %).

Vehicle emissions

The sixth source, vehicle emissions, was only identified in fine fraction and was characterized by high Pb, Cd, Zn, K and EC (Begum et al., 2004; Karnae and John, 2011). EC primarily arises from engines; Zn and K are found in tailpipe emissions; Pb is present in motor and fuel oil combustion (Yang et al., 2013). This source explained 19.6 % of $PM_{2.1}$. Contributions of vehicle emissions to $PM_{2.1}$ were higher in spring and summer. During 2000 and the period 2009–2010, the contributions from vehicles to the fine particles in Beijing were 7 and 4 %, respectively (Zheng et al., 2005; Zhang et al., 2013b), and these values are lower than those reported in this study. The source in previous studies might be primary emissions from vehicles. Besides primary emissions, however, vehicles also emit large amounts of NO_x precursors, which contributed significantly to the PM via the generation of secondary particles. This important contribution was included in the SIA source but not in the primary emissions factor. Thus, the contributions of traffic emissions to PM will be much higher than the present value if we further consider the secondary formation of NO_3^- from NO_x . Besides, vehicles equipped with three-way catalysts are an important source of NH_3 , which may also contribute to the NH_4^+ .

Mineral dust

The seventh component, mineral dust, was only identified in coarse fraction and was related to the high loading of crustal elements, such as Al, Fe, Ca (Ca^{2+}), Mg and K (K^+ ; Titos et al., 2014; Vecchi et al., 2008). This source might mainly indicate local and long-range transported dust aerosols and represented 22.6 % of the total mass in coarse fraction. It exhibited a typical seasonal variation, with higher values in spring (36.2 %).

Organic aerosol

The eighth source was relevant to organic aerosol, which was only identified in coarse fraction and was typically characterized by significant amounts of OC. Organic aerosol contributed 23.6 % ($14.7 \mu\text{g m}^{-3}$) to the coarse particles. Its contributions to $PM_{2.1-9}$ demonstrated a typical seasonal variation, with higher values in summer (51.3 %).

4.3.2 Non-haze vs. haze days

Figure 6a–d illustrate the contributions of the six sources to the fine particles and seven sources to the coarse particles on clear and haze days. On haze days, the contributions of

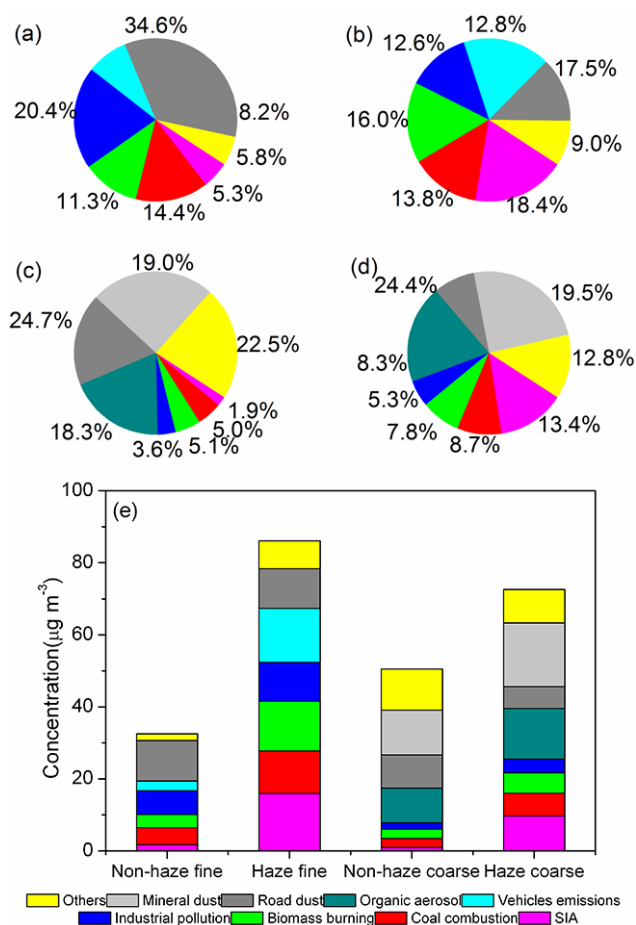


Figure 6. Relative contributions from each identified source to (a) PM_{2.1} on non-haze days, (b) PM_{2.1} on haze days, (c) PM_{2.1-9} on non-haze days, (d) PM_{2.1-9} on haze days and (e) mass concentrations of each source.

SIA, coal combustion, biomass burning, industrial pollution, road dust and vehicle emissions were 18.4, 13.8, 16.0, 12.5, 12.8 and 17.5% to the fine fractions while the contributions of SIA, coal combustion, biomass burning, industrial pollution, road dust, mineral dust and organic aerosol were 13.4, 8.7, 7.8, 5.2, 8.3, 24.4 and 19.5% to the coarse fractions. The contributions of most sources on haze days were higher than those on non-haze days, except road dust, and industrial pollution to fine fraction and mineral dust to coarse fraction particles. Additionally, the $R_{H/N}$ of the six sources was highest for SIA (6.9 to fine particles vs. 10.1 to coarse particles), followed by vehicle emissions (4.3 to fine particles), biomass burning (2.8 vs. 2.2), coal combustion (1.9 vs. 2.5), mineral dust (1.7 to coarse particles), organic aerosol (1.47 to coarse particles), industrial pollution (1.2 vs. 2.1) and, finally, road dust (0.7 vs. 0.7). The high $R_{H/N}$ values indicated that enhanced secondary conversion could occur in the atmosphere during heavy-pollution days. Furthermore, primary

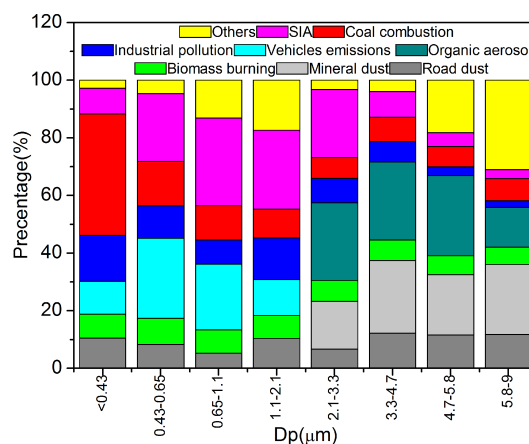


Figure 7. Relative contributions from each identified source to different size fractions.

particles and gaseous precursors from coal combustion and traffic emissions played important roles in haze pollution.

The strong contribution of mineral dust and road dust on non-haze days was primarily due to high wind speeds, which transported large quantities of particles from nearby areas within and outside of the city. Similarly, the industrial pollution affecting urban Beijing primarily arose from the surrounding areas, and the high wind speeds on non-haze days transported large quantities of industrial emission particles into Beijing from outside areas. However, on haze days, particles from coal combustion, primary emissions from vehicles, biomass burning and secondary formation were important. Thus, strict control over particles and gaseous precursor emissions from coal and oil combustion is required.

4.3.3 Differences among the size fractions

Figure 7 shows that the relative contributions of each identified source varied substantially among size fractions. Among all the sources, SIA and mineral dust (road dust for fine fractions and road dust plus mineral dust for coarse fractions), which were also identified in the mass closure analyses, exhibited relative orders in the eight size fractions that were similar to those in the mass closure results. However, the contributions of SIA in the eight size fractions were different from the contributions of SNA obtained by mass closure (i.e., 3.2–30.4% for SIA vs. 4.1–34.5% for SNA). The contribution of mineral dust increased with particle size, with the highest contribution found in the 3.3–4.7 μm fraction (37.4%) and the lowest contribution observed in the 0.65–1.1 μm fraction (5.2%). These results were consistent with the mass closure results, which indirectly verified the reliability of the PMF results.

The contributions of the other sources (coal combustion, biomass burning, industrial pollution) generally decreased with increasing size fraction; however, they exhibited peak values in both the fine and coarse modes. For example, the

contributions of coal combustion to the total mass in the different size fractions ranged from 7.2 to 42.2 %, with the highest proportion found in the $<0.43 \mu\text{m}$ fraction (42.2 %) and a relatively high proportion found in the $3.3\text{--}4.7 \mu\text{m}$ fraction (8.5 %). Similarly, the contributions of industrial pollution ranged from 2.4 (5.8–9 μm) to 15.9 % ($<0.43 \mu\text{m}$). The concentrations of biomass burning were approximately 8 % with high proportions in the fine size fractions. The complexity of the source apportionment results for different size fractions indirectly verifies that the source apportionment of $\text{PM}_{2.5}$ cannot provide comprehensive source information because it neglects the importance of the sources that dominated the coarse size fractions. For example, the highest proportion of industrial pollution was observed in the $3.3\text{--}4.7 \mu\text{m}$ size fraction.

To further examine the importance of source apportionment in the different size fractions, we compared the source apportionment results for the corresponding size sub-fractions within $\text{PM}_{2.1}$ and $\text{PM}_{2.1-9}$. As shown in Fig. 7, the contributions of each source to PM significantly varied among the size fractions within $\text{PM}_{2.1}$ and $\text{PM}_{2.1-9}$. The contributions of SIA, coal combustion, vehicle emissions and road dust to the size fractions within $\text{PM}_{2.1}$ ranged from 8.9 to 30.4 %, from 10.1 to 42.2 %, from 11.4 to 27.7 % and from 5.2 to 10.5 %, respectively. In addition, significant differences were observed among the size fractions within $\text{PM}_{2.1-9}$ regarding the contributions of SIA, industrial pollution and organic aerosol, which ranged from 3.2 to 23.6 %, from 2.4 to 8.5 % and from 13.8 to 27.9 %, respectively. This result further indicated the importance of source apportionment for subdivided size fractions within $\text{PM}_{2.1}$ and $\text{PM}_{2.1-9}$.

4.3.4 Back trajectory cluster analysis

Approximately 34 % of $\text{PM}_{2.5}$ in urban Beijing can be attributed to sources outside of Beijing, and the contribution increased to 50–70 % during sustained wind flow from southern Hebei (Streets et al., 2007). This modeling result indicated the importance of the regional transport effect on fine particles in urban Beijing. However, the regional source apportionment based on size-resolved chemical measurements was previously unavailable.

To fill this gap, the annual data were subjected to back trajectory cluster analysis to identify the source regions and primary atmospheric circulation pathways that influence the PM concentration and chemical species (Fig. 8). The air masses that reach Beijing follow seven main paths, including four from the northwest (NW, C1, C2, C5 and C7), one from the southwest (SW, C3), one from the southeast (SE, C4) and one from the northeast (NE, C6). Figure S8 shows the size distributions of the mass concentrations within each trajectory cluster. The size distributions of the mass concentrations reveal large differences between the different trajectory

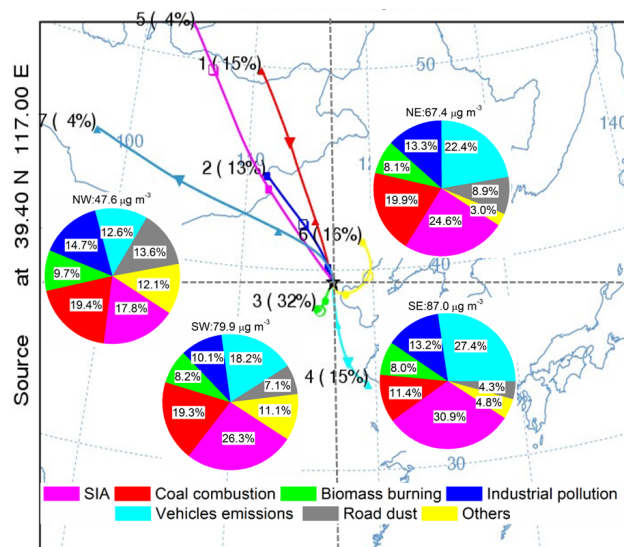


Figure 8. Relative contributions from each identified source to $\text{PM}_{2.1}$ at different trajectory clusters.

clusters in the fine mode, especially in the peak size fraction (0.65–1.1 μm).

Because regional transport has stronger impacts on fine particles than on coarse particles, with the largest differences observed between trajectory clusters, we only report the identified $\text{PM}_{2.1}$ sources associated with different trajectory clusters to determine the effects of the different source regions (Fig. 8). The polluted air mass trajectories are defined as those with $\text{PM}_{2.1}$ concentrations higher than the annual mean of $67.3 \mu\text{g m}^{-3}$.

Although the greatest proportion of the trajectories (approximately 36 %) was assigned to the NW cluster, this cluster was associated with the lowest $\text{PM}_{2.1}$ concentration of $47.6 \mu\text{g m}^{-3}$. Thus, this cluster has a weaker effect on PM pollution in Beijing. The long and rapidly moving trajectories were disaggregated into this group, and members of this cluster have extremely long transport patterns in which some parts cross over Mongolia, Inner Mongolia and northwest Hebei. In addition, this cluster was dominated by coal combustion (19 %) and SIA (18 %).

The SW cluster is the most important transport pathway with a large number of trajectories (approximately 32 %) and a high $\text{PM}_{2.1}$ concentration ($79.9 \mu\text{g m}^{-3}$). The trajectories belonging to the SW cluster are characterized by the shortest trajectories, which indicate the closest and slowest-moving air masses that are primarily transported from Hebei and south Beijing. Most of the extreme episodes in this group were probably enriched by regional and local emission sources. As shown in Fig. 8, this cluster was dominated by SIA (27 %) and coal combustion (19 %).

As shown in Fig. 8, only 15 and 16 % of the trajectories were assigned to the SE and NE clusters, respectively. However, these trajectories were associated with high $\text{PM}_{2.1}$ con-

centrations (87.0 and 67.4 $\mu\text{g m}^{-3}$). The SE cluster typically followed a flow pattern over north Jiangsu and Shandong and was dominated by SIA (31 %) and vehicle emissions (28 %). In addition, the NE cluster, which crossed over the Liaoning province and Tianjin, was dominated by SIA (25 %), vehicle emissions (22 %) and coal combustion (20 %). These results show that southern flows were dominant in urban Beijing and were associated with higher SIA, vehicle emissions and coal combustion contributions. Because SIA is primarily attributed to the transformation of precursors that originate from oil and coal combustion (i.e., NO_x and SO_2), controlling oil and coal combustion in the southern regions is required.

4.4 Reconstructing the visibility

In addition to particle size distributions, various chemical components play significant but different roles in reducing visibility on haze days. To further investigate the effects of the chemical species in the different size fractions and meteorological factors on visibility, correlation and regression analyses were performed. SPSS 16.0 was used for multiple linear regression analysis (Cheng et al., 2011).

In this study, 93 variables were investigated; however, only seven variables were selected because they had high correlation coefficients (>0.5) with visibility. Overall, the results (Table S3) showed that visibility had high correlation coefficients (>0.5) with SO_4^{2-} in the 0.43–0.65 and 0.65–1.1 μm size fractions, NH_4^+ in the 0.43–0.65 μm , NO_3^- in the 0.65–1.1 μm size fractions and Ca^{2+} in 5.8–9 μm size fraction as well as the RH and WS. All of the parameters that significantly affected visibility were used as inputs in the multiple linear regression models to simulate visibility. Ultimately, we developed the following regression equation for urban visibility in Beijing.

$$\begin{aligned} \text{Visibility} = & 13.543 - 9.214\text{RH} + 2.069\text{WS} - 0.06[\text{NH}_4^+]_{0.43-0.65} \\ & - 0.037[\text{SO}_4^{2-}]_{0.43-0.65} - 0.445[\text{SO}_4^{2-}]_{0.65-1.1} \\ & - 0.186[\text{NO}_3^-]_{0.65-1.1} - 2.18[\text{Ca}^{2+}]_{5.8-9} \end{aligned} \quad (4)$$

Previously, SO_4^{2-} , NO_3^- and NH_4^+ in $\text{PM}_{2.5}$ were reported to play important roles in visibility degradation during haze events in Beijing (Zhang et al., 2015a). Compared with previous studies, this study provides additional insights into the effects of chemical species in different size fractions on the visibility.

In addition, the RH, WS and Ca^{2+} content are important for explaining changes in visibility. High RH is conducive to the hygroscopic growth of PM and the generation of secondary species and reduces the visibility. In addition, Ca^{2+} crucially affects visibility because it associated with dust, which strongly reduces visibility. By contrast, high wind speeds are favorable for the diffusion of fine particles and can improve visibility.

NH_4^+ in the 0.43–0.65 μm size fraction, SO_4^{2-} in the 0.65–1.1 μm size fraction and NO_3^- in the 0.65–1.1 μm size fraction are also among the most important factors that affect visibility. These species primarily accumulated in the sub-micron particles. Because the SO_4^{2-} , NO_3^- and NH_4^+ in this size fraction primarily originated from gaseous precursors (NH_3 , NO_x and SO_2), regulations that control gaseous emissions of these precursors are important for reducing PM pollution and therefore improving visibility.

Our findings were similar to those reported for Jinan, in which the SO_4^{2-} and water content in the 1.0–1.8 μm fraction and the RH were the most important factors that affected visibility (Cheng et al., 2011). However, in this study, the Ca^{2+} in the coarse particles, which primarily originated from construction dust and dust transported over long distances (Liu et al., 2014a; Maenhaut et al., 2002), also played an important role in reducing the visibility in urban Beijing. However, the transport of dust over long distances is not easy to control. Thus, we stress that construction dust must be controlled to improve visibility.

To validate the above equation, size-resolved chemical species and meteorological data from other periods (from March 2012 to February 2013; Miao, 2014) were used to reconstruct the visibility using the Eq. (4). As shown in Fig. S9, the estimated visibility was well correlated with the measured visibility ($R^2 = 0.87$, $p < 0.05$). However, the ratio of the estimated visibility to the measured visibility was only 0.78, and discrete points primarily appeared for visibilities greater than 10 km (clear days). After scaling down, i.e., using data sets with visibilities less than 10 km to reconstruct the visibility, the ratio of the estimated visibility to the measured visibility reached 1.15 and R^2 reached 0.97. This result indicated that parameters in Eq. (4) affecting visibility were different for haze and clear conditions. There is also another indication that the above equation can characterize the relationship between visibility and chemical species during haze periods with a visibility of less than 10 km. A similar equation will be useful for further reconstructing the relationships between visibility and PM source and we will do more discussion regarding this topic in the future.

5 Summary and conclusions

The analysis of size-segregated airborne particles collected in Beijing from 1 March 2013 to 28 February 2014 was presented. The annual average mass concentrations of the fine and coarse particles were higher than the National Ambient Air Quality Standard (Grade I) of China. The OC, SO_4^{2-} , NO_3^- and NH_4^+ species were the most abundant in the fine particles, accounting for 24.5, 14.7, 11.2 and 9.2 % of the $\text{PM}_{2.1}$ mass, respectively. In $\text{PM}_{2.1-9}$, the primary chemical components were Ca (16.3 %) and OC (15.5 %). SOC, which formed due to photochemical reactions, primarily accumulated in the “condensation mode”. The size distribution of the

OC peaked at 0.43–0.65 μm in summer and at 0.65–1.1 μm in winter.

The data set excluding extreme weather events (i.e., rain, snow, fog and dust) was categorized into non-haze and haze days. NO_3^- , SO_4^{2-} , NH_4^+ , Pb, Tl and Cd in $\text{PM}_{2.1}$ accumulated heavily during haze periods with $R_{\text{H/N}} > 2.6$. In coarse particles, the $R_{\text{H/N}}$ values of NH_4^+ , NO_3^- , SO_4^{2-} , Cd, EC, Cl^- , Pb, Tl, Na^+ , OC, Zn and K^+ were also greater than unity, indicating that the effect of particles with a diameter larger than 2.1 μm cannot be neglected. The annual average size distributions of SO_4^{2-} , OC, NO_3^- , NH_4^+ , Cl^- , K^+ and Cd exhibited peak shifts from 0.43–0.65 μm on non-haze days to 0.65–1.1 μm on haze days. In addition, a regression equation was developed to characterize the relationship between the visibility and the chemical species concentrations and meteorological data when the visibility was less than 10 km.

The mass closure results showed that OM, SNA and CM dominated the fine and coarse particulate mass concentrations. Although OM dominated in fine particles, it decreased from 37.9% on non-haze days to 31.2% on haze days. In contrast, the contribution of SNA to the $\text{PM}_{2.1}$ mass increased from 19.1% on non-haze days to 33.9% on haze days, indicating that SNA played a key role in haze formation. Moreover, the contributions of SNA, OM, HM and EC decreased as the size increased, whereas those of CM and SS exhibited the opposite trend. Further studies are required to determine the identities of the unidentified components in the larger size fractions.

Six $\text{PM}_{2.1}$ sources and seven $\text{PM}_{2.1-9}$ sources were identified using the PMF method based on 1-year size-segregated data. The sources' contributions varied between non-haze and haze days. The results show that coal combustion, vehicle emissions, industrial pollution, biomass burning and secondary formation were major contributors on haze days. In contrast, mineral dust (road dust) was important source on non-haze days. In addition, the relative contributions of these sources in Beijing varied significantly as the fraction sizes changed. The contributions of all of the sources decreased as the size of the fraction increased with the exception of mineral dust; however, they exhibited relatively high proportions in the fine and coarse modes, indicating the importance of source apportionment for size sub-fractions within $\text{PM}_{2.1}$ and $\text{PM}_{2.1-9}$. Combining these findings with the trajectory clustering results, the source regions associated with $\text{PM}_{2.1}$ in Beijing were further explored. We found that the southern and northeastern flows are associated with greater SIA, vehicle emissions and coal combustion contributions, whereas the northwestern flows transport more mineral dust.

The Supplement related to this article is available online at doi:10.5194/acp-16-1-2016-supplement.

Acknowledgements. This study supported by the “Strategic Priority Research Program” of the Chinese Academy of Sciences (XDB05020000 and XDA05100100) the National Natural Science Foundation of China (nos. 41405144, 41230642 and 41321064) and Haze Observation Project especially for Jing–Jin–Ji area (HOPE-J³A; no. KJZD-EW-TZ-G06-01-04).

Edited by: M. Shao

References

- Begum, B. A., Kim, E., Biswas, S. K., and Hopke, P. K.: Investigation of sources of atmospheric aerosol at urban and semi-urban areas in Bangladesh, *Atmos. Environ.*, 38, 3025–3038, doi:10.1016/j.atmosenv.2004.02.042, 2004.
- Bullock, K. R., Duvall, R. M., Norris, G. A., McDow, S. R., and Hays, M. D.: Evaluation of the CMB and PMF models using organic molecular markers in fine particulate matter collected during the Pittsburgh Air Quality Study, *Atmos. Environ.*, 42, 6897–6904, doi:10.1016/j.atmosenv.2008.05.011, 2008.
- Cao, J., Lee, S., Chow, J. C., Watson, J. G., Ho, K., Zhang, R., Jin, Z., Shen, Z., Chen, G., and Kang, Y.: Spatial and seasonal distributions of carbonaceous aerosols over China, *J. Geophys. Res.*, 112, D22S11, doi:10.1029/2006JD008205, 2007.
- Chan, C. Y., Xu, X. D., Li, Y. S., Wong, K. H., Ding, G. A., Chan, L. Y., and Cheng, X. H.: Characteristics of vertical profiles and sources of $\text{PM}_{2.5}$, PM_{10} and carbonaceous species in Beijing, *Atmos. Environ.*, 39, 5113–5124, doi:10.1016/j.atmosenv.2005.05.009, 2005.
- Cheng, S.-h., Yang, L.-x., Zhou, X.-h., Xue, L.-k., Gao, X.-m., Zhou, Y., and Wang, W.-X.: Size-fractionated water-soluble ions, situ pH and water content in aerosol on hazy days and the influences on visibility impairment in Jinan, China, *Atmos. Environ.*, 45, 4631–4640, doi:10.1016/j.atmosenv.2011.05.057, 2011.
- Cheng, Y., Engling, G., He, K. B., Duan, F. K., Du, Z. Y., Ma, Y. L., Liang, L. L., Lu, Z. F., Liu, J. M., Zheng, M., and Weber, R. J.: The characteristics of Beijing aerosol during two distinct episodes: Impacts of biomass burning and fireworks, *Environ. Pollut.*, 185, 149–157, doi:10.1016/j.envpol.2013.10.037, 2014.
- Contini, D., Cesari, D., Genga, A., Siciliano, M., Ielpo, P., Guascito, M. R., and Conte, M.: Source apportionment of size-segregated atmospheric particles based on the major water-soluble components in Lecce (Italy), *Sci. Total Environ.*, 472, 248–261, doi:10.1016/j.scitotenv.2013.10.127, 2014.
- Du, H., Kong, L., Cheng, T., Chen, J., Du, J., Li, L., Xia, X., Leng, C., and Huang, G.: Insights into summertime haze pollution events over Shanghai based on online water-soluble ionic composition of aerosols, *Atmos. Environ.*, 45, 5131–5137, doi:10.1016/j.atmosenv.2011.06.027, 2011.
- Du, Z., He, K., Cheng, Y., Duan, F., Ma, Y., Liu, J., Zhang, X., Zheng, M., and Weber, R.: A year long study of water-soluble organic carbon in Beijing II: Light absorption properties, *Atmos. Environ.*, 89, 235–241, doi:10.1016/j.atmosenv.2014.02.022, 2014.
- Duan, F., He, K., Ma, Y., Jia, Y., Yang, F., Lei, Y., Tanaka, S., and Okuta, T.: Characteristics of carbonaceous aerosols in Beijing, China, *Chemosphere*, 60, 355–364, doi:10.1016/j.chemosphere.2004.12.035, 2005.

- Duarte, R. M. B. O., Mieiro, C. L., Penetra, A., Pio, C. A., and Duarte, A. C.: Carbonaceous materials in size-segregated atmospheric aerosols from urban and coastal-rural areas at the Western European Coast, *Atmos. Res.*, 90, 253–263, doi:10.1016/j.atmosres.2008.03.003, 2008.
- Fisher, J. A., Jacob, D. J., Wang, Q., Bahreini, R., Carouge, C. C., Cubison, M. J., Dibb, J. E., Diehl, T., Jimenez, J. L., Leibensperger, E. M., Lu, Z., Meinders, M. B. J., Pye, H. O. T., Quinn, P. K., Sharma, S., Streets, D. G., van Donkelaar, A., and Yantosca, R. M.: Sources, distribution, and acidity of sulfate–ammonium aerosol in the Arctic in winter–spring, *Atmos. Environ.*, 45, 7301–7318, doi:10.1016/j.atmosenv.2011.08.030, 2011.
- Gao, J., Chai, F., Wang, T., Wang, S., and Wang, W.: Particle number size distribution and new particle formation: New characteristics during the special pollution control period in Beijing, *J. Environ. Sci.*, 24, 14–21, doi:10.1016/S1001-0742(11)60725-0, 2012.
- Guo, S., Hu, M., Wang, Z. B., Slanina, J., and Zhao, Y. L.: Size-resolved aerosol water-soluble ionic compositions in the summer of Beijing: implication of regional secondary formation, *Atmos. Chem. Phys.*, 10, 947–959, doi:10.5194/acp-10-947-2010, 2010.
- Guo, S., Hu, M., Zamora, M. L., Peng, J., Shang, D., Zheng, J., Du, Z., Wu, Z., Shao, M., Zeng, L., Molina, M. J., and Zhang, R.: Elucidating severe urban haze formation in China, *P. Natl. Acad. Sci. USA*, 111, 17373–17378, doi:10.1073/pnas.1419604111, 2014.
- Hou, B., Zhuang, G., Zhang, R., Liu, T., Guo, Z., and Chen, Y.: The implication of carbonaceous aerosol to the formation of haze: Revealed from the characteristics and sources of OC/EC over a mega-city in China, *J. Hazard. Mater.*, 190, 529–536, doi:10.1016/j.jhazmat.2011.03.072, 2011.
- Huang, R. J., Zhang, Y. L., Bozzetti, C., Ho, K. F., Cao, J. J., Han, Y. M., Daellenbach, K. R., Slowik, J. G., Platt, S. M., Canonaco, F., Zotter, P., Wolf, R., Pieber, S. M., Bruns, E. A., Crippa, M., Ciarelli, G., Piazzalunga, A., Schwikowski, M., Abbazade, G., Schnelle-Kreis, J., Zimmermann, R., An, Z. S., Szidat, S., Baltensperger, U., El Haddad, I., and Prevot, A. S. H.: High secondary aerosol contribution to particulate pollution during haze events in China, *Nature*, 514, 218–222, doi:10.1038/nature13774, 2014.
- Hueglin, C., Gehrig, R., Baltensperger, U., Gysel, M., Monn, C., and Vonmont, H.: Chemical characterisation of PM_{2.5}, PM₁₀ and coarse particles at urban, near-city and rural sites in Switzerland, *Atmos. Environ.*, 39, 637–651, doi:10.1016/j.atmosenv.2004.10.027, 2005.
- Jacobson, M. C., Hansson, H. C., Noone, K. J., and Charlson, R. J.: Organic atmospheric aerosols: Review and state of the science, *Rev. Geophys.*, 38, 267–294, doi:10.1029/1998rg000045, 2000.
- Jing, H., Li, Y.-F., Zhao, J., Li, B., Sun, J., Chen, R., Gao, Y., and Chen, C.: Wide-range particle characterization and elemental concentration in Beijing aerosol during the 2013 Spring Festival, *Environ. Pollut.*, 192, 204–211, doi:10.1016/j.envpol.2014.06.003, 2014.
- Kang, J., Choi, M.-S., Yi, H.-I., Song, Y.-H., Lee, D., and Cho, J.-H.: A five-year observation of atmospheric metals on Ulleung Island in the East/Japan Sea: Temporal variability and source identification, *Atmos. Environ.*, 45, 4252–4262, doi:10.1016/j.atmosenv.2011.04.083, 2011.
- Karanasiou, A. A., Siskos, P. A., and Eleftheriadis, K.: Assessment of source apportionment by Positive Matrix Factorization analysis on fine and coarse urban aerosol size fractions, *Atmos. Environ.*, 43, 3385–3395, doi:10.1016/j.atmosenv.2009.03.051, 2009.
- Karnaes, S. and John, K.: Source apportionment of fine particulate matter measured in an industrialized coastal urban area of South Texas, *Atmos. Environ.*, 45, 3769–3776, doi:10.1016/j.atmosenv.2011.04.040, 2011.
- Li, X., Wang, L., Wang, Y., Wen, T., Yang, Y., Zhao, Y., and Wang, Y.: Chemical composition and size distribution of airborne particulate matters in Beijing during the 2008 Olympics, *Atmos. Environ.*, 50, 278–286, doi:10.1016/j.atmosenv.2011.12.021, 2012.
- Li, X., Wang, L., Ji, D., Wen, T., Pan, Y., Sun, Y., and Wang, Y.: Characterization of the size-segregated water-soluble inorganic ions in the Jing-Jin-Ji urban agglomeration: Spatial/temporal variability, size distribution and sources, *Atmos. Environ.*, 77, 250–259, doi:10.1016/j.atmosenv.2013.03.042, 2013.
- Liu, Q., Liu, Y., Yin, J., Zhang, M., and Zhang, T.: Chemical characteristics and source apportionment of PM₁₀ during Asian dust storm and non-dust storm days in Beijing, *Atmos. Environ.*, 91, 85–94, doi:10.1016/j.atmosenv.2014.03.057, 2014a.
- Liu, S., Hu, M., Slanina, S., He, L. Y., Niu, Y. W., Brüegemann, E., Gnauk, T., and Herrmann, H.: Size distribution and source analysis of ionic compositions of aerosols in polluted periods at Xinken in Pearl River Delta (PRD) of China, *Atmos. Environ.*, 42, 6284–6295, doi:10.1016/j.atmosenv.2007.12.035, 2008.
- Liu, Z. R., Hu, B., Liu, Q., Sun, Y., and Wang, Y. S.: Source apportionment of urban fine particle number concentration during summertime in Beijing, *Atmos. Environ.*, 359–369, doi:10.1016/j.atmosenv.2014.06.055, 2014b.
- Maenhaut, W., Cafmeyer, J., Dubtsov, S., and Chi, X.: Detailed mass size distributions of elements and species, and aerosol chemical mass closure during fall 1999 at Gent, Belgium, *Nucl. Instrum. Meth. B*, 189, 238–242, doi:10.1016/s0168-583x(01)01049-7, 2002.
- McFiggans, G.: Atmospheric science Involatile particles from rapid oxidation, *Nature*, 506, 442–443, doi:10.1038/506442a, 2014.
- Miao, H.: Spatial and temporal characterizations of water soluble inorganic ions of aerosol in China, *Institute of Atmosphere Physics, Chinese Academy of Science, Beijing*, 57–76, 2014.
- Moon, K. J., Han, J. S., Ghim, Y. S., and Kim, Y. J.: Source apportionment of fine carbonaceous particles by positive matrix factorization at Gosan background site in East Asia, *Environ. Int.*, 34, 654–664, doi:10.1016/j.envint.2007.12.021, 2008.
- Paatero, P.: Least square formulation of robust non-negative factor analysis, *Chemometr. Intell. Lab.*, 3, 23–35, doi:10.1016/S0169-7439(96)00044-5, 1997.
- Paatero, P. and Tapper, U.: Positive matrix factorization: A non-negative factor model with optimal utilization of error estimates of data values, *Environmetrics*, 5, 111–126, doi:10.1002/env.3170050203, 1994.
- Pan, Y. P. and Wang, Y. S.: Atmospheric wet and dry deposition of trace elements at 10 sites in Northern China, *Atmos. Chem. Phys.*, 15, 951–972, doi:10.5194/acp-15-951-2015, 2015.
- Pan, Y. P., Wang, Y. S., Tang, G. Q., and Wu, D.: Spatial distribution and temporal variations of atmospheric sulfur deposition in Northern China: insights into the potential acidification risks, *Atmos. Chem. Phys.*, 13, 1675–1688, doi:10.5194/acp-13-1675-2013, 2013.

- Pant, P. and Harrison, R. M.: Critical review of receptor modelling for particulate matter: A case study of India, *Atmos. Environ.*, 49, 1–12, doi:10.1016/j.atmosenv.2011.11.060, 2012.
- Pillai, P. S. and Moorthy, K. K.: Aerosol mass-size distributions at a tropical coastal environment: response to mesoscale and synoptic processes, *Atmos. Environ.*, 35, 4099–4112, doi:10.1016/s1352-2310(01)00211-4, 2001.
- Quan, J., Tie, X., Zhang, Q., Liu, Q., Li, X., Gao, Y., and Zhao, D.: Characteristics of heavy aerosol pollution during the 2012–2013 winter in Beijing, China, *Atmos. Environ.*, 88, 83–89, doi:10.1016/j.atmosenv.2014.01.058, 2014.
- Schleicher, N., Norra, S., Fricker, M., Kaminski, U., Chen, Y., Chai, F., Wang, S., Yu, Y., and Cen, K.: Spatio-temporal variations of black carbon concentrations in the Megacity Beijing, *Environ. Pollut.*, 182, 392–401, doi:10.1016/j.envpol.2013.07.042, 2013.
- Sirois, A. and Bottenheim, J. W.: Use of backward trajectories to interpret the 5-year record of PAN and O₃ ambient air concentrations at Kejimikujik National Park, Nova Scotia, *J. Geophys. Res.*, 100, 2867–2881, doi:10.1029/94jd02951, 1995.
- Song, Y., Zhang, Y., Xie, S., Zeng, L., Zheng, M., Salmon, L. G., Shao, M., and Slanina, S.: Source apportionment of PM_{2.5} in Beijing by positive matrix factorization, *Atmos. Environ.*, 40, 1526–1537, doi:10.1016/j.atmosenv.2005.10.039, 2006.
- Song, Y., Tang, X., Xie, S., Zhang, Y., Wei, Y., Zhang, M., Zeng, L., and Lu, S.: Source apportionment of PM_{2.5} in Beijing in 2004, *J. Hazard. Mater.*, 146, 124–130, doi:10.1016/j.jhazmat.2006.11.058, 2007.
- Streets, D. G., Fu, J. S., Jang, C. J., Hao, J., He, K., Tang, X., Zhang, Y., Wang, Z., Li, Z., Zhang, Q., Wang, L., Wang, B., and Yu, C.: Air quality during the 2008 Beijing Olympic Games, *Atmos. Environ.*, 41, 480–492, doi:10.1016/j.atmosenv.2006.08.046, 2007.
- Sun, J., Zhang, Q., Canagaratna, M. R., Zhang, Y., Ng, N. L., Sun, Y., Jayne, J. T., Zhang, X., Zhang, X., and Worsnop, D. R.: Highly time- and size-resolved characterization of submicron aerosol particles in Beijing using an Aerodyne Aerosol Mass Spectrometer, *Atmos. Environ.*, 44, 131–140, doi:10.1016/j.atmosenv.2009.03.020, 2010.
- Sun, Y., Zhuang, G., Wang, Y., Han, L., Guo, J., Dan, M., Zhang, W., Wang, Z., and Hao, Z.: The air-borne particulate pollution in Beijing – concentration, composition, distribution and sources, *Atmos. Environ.*, 38, 5991–6004, doi:10.1016/j.atmosenv.2004.07.009, 2004.
- Sun, Y., Zhuang, G., Tang, A., Wang, Y., and An, Z.: Chemical characteristics of PM_{2.5} and PM₁₀ in haze-fog episodes in Beijing, *Environ. Sci. Technol.*, 40, 3148–3155, 2006.
- Sun, Z., Mu, Y., Liu, Y., and Shao, L.: A comparison study on airborne particles during haze days and non-haze days in Beijing, *Sci. Total Environ.*, 456–457, 1–8, doi:10.1016/j.scitotenv.2013.03.006, 2013.
- Tan, J. H., Duan, J. C., Chen, D. H., Wang, X. H., Guo, S. J., Bi, X. H., Sheng, G. Y., He, K. B., and Fu, J. M.: Chemical characteristics of haze during summer and winter in Guangzhou, *Atmos. Res.*, 94, 238–245, doi:10.1016/j.atmosres.2009.05.016, 2009.
- Tian, H. Z., Wang, Y., Xue, Z. G., Cheng, K., Qu, Y. P., Chai, F. H., and Hao, J. M.: Trend and characteristics of atmospheric emissions of Hg, As, and Se from coal combustion in China, 1980–2007, *Atmos. Chem. Phys.*, 10, 11905–11919, doi:10.5194/acp-10-11905-2010, 2010.
- Tian, S., Pan, Y., Liu, Z., Wen, T., and Wang, Y.: Size-resolved aerosol chemical analysis of extreme haze pollution events during early 2013 in urban Beijing, China, *J. Hazard. Mater.*, 279, 452–460, doi:10.1016/j.jhazmat.2014.07.023, 2014.
- Titos, G., Lyamani, H., Pandolfi, M., Alastuey, A., and Alados-Arboledas, L.: Identification of fine (PM₁) and coarse (PM_{10–1}) sources of particulate matter in an urban environment, *Atmos. Environ.*, 89, 593–602, doi:10.1016/j.atmosenv.2014.03.001, 2014.
- Vecchi, R., Chiari, M., D’Alessandro, A., Fermo, P., Lucarelli, F., Mazzei, F., Nava, S., Piazzalunga, A., Prati, P., Silvani, F., and Valli, G.: A mass closure and PMF source apportionment study on the sub-micron sized aerosol fraction at urban sites in Italy, *Atmos. Environ.*, 42, 2240–2253, doi:10.1016/j.atmosenv.2007.11.039, 2008.
- Wang, G., Kawamura, K., Lee, S., Ho, K., and Cao, J.: Molecular, Seasonal, and Spatial Distributions of Organic Aerosols from Fourteen Chinese Cities, *Environ. Sci. Technol.*, 40, 4619–4625, doi:10.1021/es060291x, 2006a.
- Wang, L., Xin, J., Li, X., and Wang, Y.: The variability of biomass burning and its influence on regional aerosol properties during the wheat harvest season in North China, *Atmos. Res.*, 157, 153–163, doi:10.1016/j.atmosres.2015.01.009, 2015.
- Wang, L. T., Wei, Z., Yang, J., Zhang, Y., Zhang, F. F., Su, J., Meng, C. C., and Zhang, Q.: The 2013 severe haze over southern Hebei, China: model evaluation, source apportionment, and policy implications, *Atmos. Chem. Phys.*, 14, 3151–3173, doi:10.5194/acp-14-3151-2014, 2014.
- Wang, X., Wang, W., Yang, L., Gao, X., Nie, W., Yu, Y., Xu, P., Zhou, Y., and Wang, Z.: The secondary formation of inorganic aerosols in the droplet mode through heterogeneous aqueous reactions under haze conditions, *Atmos. Environ.*, 63, 68–76, doi:10.1016/j.atmosenv.2012.09.029, 2012.
- Wang, Y. Q., Zhang, X. Y., and Arimoto, R.: The contribution from distant dust sources to the atmospheric particulate matter loadings at XiAn, China during spring, *Sci. Total Environ.*, 368, 875–883, doi:10.1016/j.scitotenv.2006.03.040, 2006b.
- Yan, C., Zheng, M., Sullivan, A. P., Bosch, C., Desyaterik, Y., Andersson, A., Li, X., Guo, X., Zhou, T., Gustafsson, Ö., and Collett Jr, J. L.: Chemical characteristics and light-absorbing property of water-soluble organic carbon in Beijing: Biomass burning contributions, *Atmos. Environ.*, 121, 4–12, doi:10.1016/j.atmosenv.2015.05.005, 2015.
- Yang, L., Cheng, S., Wang, X., Nie, W., Xu, P., Gao, X., Yuan, C., and Wang, W.: Source identification and health impact of PM_{2.5} in a heavily polluted urban atmosphere in China, *Atmos. Environ.*, 75, 265–269, doi:10.1016/j.atmosenv.2013.04.058, 2013.
- Yang, X., Chen, Y. Z., Liu, H. F., Zhao, Y. X., Gao, J., Chai, F. H., and Meng, F.: Characteristics and formation mechanism of a serious haze event in January 2013 in Beijing, China *Environ. Sci.*, 34, 282–288, 2014.
- Yang, Y., Wang, Y., Wen, T., Wei, L., Ya’nan, Z., and Liang, L.: Elemental composition of PM_{2.5} and PM₁₀ at Mount Gongga in China during 2006, *Atmos. Res.*, 93, 801–810, doi:10.1016/j.atmosres.2009.03.014, 2009.
- Yao, X., Lau, A. P. S., Fang, M., Chan, C. K., and Hu, M.: Size distributions and formation of ionic species in atmospheric particulate pollutants in Beijing, China: inorganic ions, *Atmos.*

- Environ., 37, 2991–3000, doi:10.1016/S1352-2310(03)00255-3, 2003.
- Zhang, G., Bi, X., Chan, L. Y., Wang, X., Sheng, G., and Fu, J.: Size-segregated chemical characteristics of aerosol during haze in an urban area of the Pearl River Delta region, China, *Urban Clim.*, 4, 74–84, doi:10.1016/j.uclim.2013.05.002, 2013a.
- Zhang, H., Hu, J., Kleeman, M., and Ying, Q.: Source apportionment of sulfate and nitrate particulate matter in the Eastern United States and effectiveness of emission control programs, *Sci. Total Environ.*, 490, 171–181, doi:10.1016/j.scitotenv.2014.04.064, 2014a.
- Zhang, J. K., Sun, Y., Liu, Z. R., Ji, D. S., Hu, B., Liu, Q., and Wang, Y. S.: Characterization of submicron aerosols during a month of serious pollution in Beijing, 2013, *Atmos. Chem. Phys.*, 14, 2887–2903, doi:10.5194/acp-14-2887-2014, 2014b.
- Zhang, Q., Quan, J., Tie, X., Li, X., Liu, Q., Gao, Y., and Zhao, D.: Effects of meteorology and secondary particle formation on visibility during heavy haze events in Beijing, China, *Sci. Total Environ.*, 502, 578–584, doi:10.1016/j.scitotenv.2014.09.079, 2015a.
- Zhang, R., Suh, I., Zhao, J., Zhang, D., Fortner, E. C., Tie, X., Molina, L. T., and Molina, M. J.: Atmospheric new particle formation enhanced by organic acids, *Science*, 304, 1487–1490, 2004.
- Zhang, R., Khalizov, A., Wang, L., Hu, M., and Xu, W.: Nucleation and growth of nanoparticles in the atmosphere, *Chem. Rev.*, 112, 1957–2011, 2011.
- Zhang, R., Jing, J., Tao, J., Hsu, S.-C., Wang, G., Cao, J., Lee, C. S. L., Zhu, L., Chen, Z., Zhao, Y., and Shen, Z.: Chemical characterization and source apportionment of PM_{2.5} in Beijing: seasonal perspective, *Atmos. Chem. Phys.*, 13, 7053–7074, doi:10.5194/acp-13-7053-2013, 2013b.
- Zhang, R., Wang, G., Guo, S., Zamora, M. L., Ying, Q., Lin, Y., Wang, W., Hu, M., and Wang, Y.: Formation of Urban Fine Particulate Matter, *Chem. Rev.*, 115, 3803–3855, doi:10.1021/acs.chemrev.5b00067, 2015b.
- Zhang, W., Zhuang, G., Guo, J., Xu, D., Wang, W., Baumgardner, D., Wu, Z., and Yang, W.: Sources of aerosol as determined from elemental composition and size distributions in Beijing, *Atmos. Res.*, 95, 197–209, doi:10.1016/j.atmosres.2009.09.017, 2010.
- Zhang, X. Y., Wang, Y. Q., Zhang, X. C., Guo, W., and Gong, S. L.: Carbonaceous aerosol composition over various regions of China during 2006, *J. Geophys. Res.*, 113, D14111, doi:10.1029/2007jd009525, 2008.
- Zheng, M., Salmon, L. G., Schauer, J. J., Zeng, L., Kiang, C., Zhang, Y., and Cass, G. R.: Seasonal trends in PM_{2.5} source contributions in Beijing, China, *Atmos. Environ.*, 39, 3967–3976, 2005.
- Zhuang, X., Wang, Y., He, H., Liu, J., Wang, X., Zhu, T., Ge, M., Zhou, J., Tang, G., and Ma, J.: Haze insights and mitigation in China: An overview, *J. Environ. Sci.*, 26, 2–12, doi:10.1016/S1001-0742(13)60376-9, 2014.